Constitutive Plasma Membrane Turnover in T-REx293 cells via Ordered Membrane Domain Endocytosis under Mitochondrial Control

Christine Deisl[1], Orson W. Moe, and Donald W. Hilgemann

Department of Physiology, University of Texas Southwestern Medical Center, Dallas, Texas, USA

Department of Internal Medicine, University of Texas Southwestern Medical Center, Dallas, Texas, USA

Charles and Jane Pak Center for Mineral Metabolism and Clinical Research, University of Texas Southwestern Medical Center, Dallas, Texas, USA

[1]Present address: Institute of Anatomy and Cell Biology, Paracelsus Medical University, Salzburg, Austria

Corresponding author: Donald W. Hilgemann

Correspondence to: donald.hilgemann@utsouthwestern.edu

Abstract.

Clathrin/dynamin-independent endocytosis of ordered plasma membrane domains (**o**rdered **m**embrane **d**omain **e**ndocytosis, OMDE) can be far more powerful than conventional endocytosis. Nevertheless, it remains controversial how OMDE takes place, in which cell processes it is important, and how it is regulated. Using patch clamp, we have described that OMDE becomes massive in multiple cell types in response to Ca elevations, G protein activation by non-hydrolyzable GTP analogs, and enhanced oxidative metabolism. We describe here that cytoplasmic succinate and pyruvate, but not β-hydroxybutyrate, can induce OMDE of 75% of the plasma membrane in murine marrow macrophages (BMMs) within 2 min. OMDE is decreased by 70% in BMMs lacking the acyltransferase, DHHC5, by treatment with carnitine to shift long-chain acyl groups from cytoplasmic to mitochondrial acyl-CoA's, by bromopalmitate/albumin complexes to block DHHCs, and by the cyclosporin, NIM811, to block permeability transition pores that may release mitochondrial coenzyme A into the cytoplasm. Using T-REx293 cells, plasma membrane loss amounts to 40% with pyruvate or GTPγS, whereby OMDE is then highly sensitive to actin cytoskeleton disruption. Using fluorescent 3kD dextrans to monitor constitutive endocytosis in unperturbed cells without serum or bicarbonate, multiple results suggest that OMDE is constitutively active in T-REx293 cells, but not in BMMs. In T-REx293 cells, substrates that generate metabolites activated by coenyzme A (CoA), e.g. pyruvate and hydroxybutyrate, inhibit endocytosis as expected for a shift of long-chain acyl-CoA to other CoA metabolites. In the presence of bicarbonate, however, pyruvate strongly enhances OMDE, and OMDE is then blocked by β-hydroxybutyrate, bromopalmitate/albumin complexes, and cyclosporines. After pyruvate responses, T-REx293 cells grow normally without evidence of apoptosis. Low concentrations of fatty acid (FA)-free albumin inhibit basal endocytosis in T-REx293 cells, but not BMMs, as do cyclosporines, carnitine, and RhoA blockade. However, constitutive endocytosis (i.e. in the absence of substrates and bicarbonate) is not inhibited by siRNA knockdown of the acyltransferases, DHHC5 or DHHC2, which support OMDE responses activated in patch clamp experiments. We verify biochemically that small CoA metabolites cause a decrease of long-chain acyl-CoA's and that several palmitoylated membrane proteins are depalmitoylated during treatments that decrease long-chain acyl-CoA's. STED microscopy reveals that vesicles formed in constitutive OMDE in T-REX293 cells have diameters of 90 to 130 nm. In summary, palmitoylation-dependent OMDE is likely a major G-protein-dependent endocytic mechanism that can be constitutively active, albeit not in BMMs. It depends on the activities of different DHHC acyltransferases in different cellular circumstances and can be limited by local supplies of fatty acids, CoA, and long-chain acyl-CoA's.

Abbreviations.

bone marrow macrophages (BBMs), bromopalmitate (BP), cholera toxin B (CTB), coenzyme A (CoA), cyclosporine A (CsA), fatty acid (FA), β-hydroxybutyrate (β-HB), ordered membrane domain endocytosis (OMDE), permeability transition pores (PTPs), plasma membrane (PM), reactive oxygen species (ROS), transferrin (TF).

Introduction.

Eukaryotic cells use endocytosis (1, 2) to carry out a wide range of cellular functions. Phagocytosis and macropinocytosis are used to internalize large particles and fluid volumes (3). Micro-pinocytotic mechanisms generate vesicles from the plasma membrane (PM) with diameters of 40 to 200 nm (4), thereby internalizing integral PM proteins, PM-associated proteins, and various other types of particles, as well fluid (5). In doing so, micro-pinocytotic mechanisms re-localize membrane and membrane proteins from the cell surface into the secretory pathway for recycling, degradation, and cell signaling functions. Innumerable studies document that micro-pinocytosis occurs by diverse mechanisms, ranging from the coordinated operation of clathrin, dynamins, and other adapter proteins, to the lateral reorganization of plasma membrane lipids and proteins into domains, often with additional involvements of actin cytoskeleton to direct budding and vesiculation (6). Dynamins are known to drive some forms of endocytosis without clathrin (7). However, one such example has recently been contradicted. In contrast to a long-time assumption of the field, it was recently shown that dynamin-2 does not support the clathrin-independent internalization of caveolae, but rather restrains caveolae internalization (8). Another instructive example of complexity concerns turnover of PM in two cell types used routinely in cell biological studies. For HeLa cells, it is proposed that nearly all PM turnover under standard cell culture conditions occurs via clathrin/dynamin-dependent mechanisms (9). In mouse fibroblasts, by contrast, the deletion of all three dynamins results in no evident change of fluid phase endocytosis (10), and we verify this result in Supplemental Fig. S1. Importantly, analysis of fluid phase dextran uptake by confocal optical methods can indeed readily detect clathrin/dynamin endocytosis (e.g.(11)). Thus, it remains to be established whether (i) different endocytic mechanisms operate drastically differently in different cell types, (ii) different endocytic mechanisms compensate one another when one is manipulated by genetic means, or whether (iii) clathrin/dynamin endocytosis represents only a small fraction of PM turnover in fibroblasts.

Using patch clamp to monitor PM area changes and to manipulate contents of the cytoplasm, we have been impressed by the large magnitudes and speeds with which endocytic responses can occur via clathrin/dynamin-independent mechanisms (12). We have documented in multiple cell types the occurrence of massive endocytosis that can internalize more than 50% of the PM into relatively small vesicles (i.e. less than 240 nm) within one to two minutes (12). We have documented these responses to occur in primarily three circumstances—in the wake of cytoplasmic Ca elevations, during activation of G- proteins by nonhydrolyzable GTP analogs and the activation of oxidative phosphorylation in mitochondria by substrates such as succinate. In all cases, we have verified that the membrane that internalizes binds amphipathic compounds less well than membrane that remains at the cell surface.

Given that more ordered membrane domains internalize, we suggest that this form of endocytosis may productively be called ordered membrane domain endocytosis (OMDE). This term can then be used to include coherently the various forms of endocytoses otherwise called 'raft' (13), 'CLIC' (14) and 'bulk' (15) endocytosis. All of these endocytic mechanisms are dynamin/clathrin-independent and have variable dependence on actin cytoskeleton function in addition to membrane lipid and protein ordering.

While patch clamp results suggest that OMDE can be remarkably powerful when activated, available data does not establish that OMDE is active constitutively in cells or under standard cell culture conditions. Rather, work to date indicates that OMDE becomes active under specific cellular conditions that promote palmitoylation of membrane proteins which can subsequently coalesce into ordered domains. As already noted, this appears to occur in dependence on mitochondrial oxidative stress, and some details are outlined in cartoon form in Fig. 1. In brief, mitochondria accumulate the ubiquitous enzymatic cofactor, coenzyme A (CoA), to high concentrations with respect to the cytoplasm (16, 17). As mitochondria generate reactive oxygen species (ROS) associated with enhanced cytochrome oxidase activities and Ca accumulation, the transient opening of permeability transition pores (PTPs) allows coenzyme A to escape to the cytoplasm, promoting generation of long-chain acyl-CoAs. In dependence on acyl-CoA accumulation, as well as other signaling mechanisms that are only partially elucidated, key PM proteins are evidently rapidly palmitoylated to promote OMDE. To address the possible constitutive function of OMDE, we describe here studies of fluid phase endocytosis of small fluorescent dextrans (3-10 kD) in cultured cells in which we have tested acute effects of factors that promote or hinder OMDE in patch clamp experiments. Further to this end, we compare the function of endocytosis in two very different cell types, T-REx293 cells and differentiated murine bone marrow macrophages (BMMs).

To summarize the scope of this article, we show first via patch clamp that OMDE activated by oxidative metabolism in BMMs is more powerful than in other cells, internalizing 75% of the PM in 2 min and requiring expression of the acyltransferase, DHHC5. While less powerful, we show that OMDE activated by GTPγS in T-REx293 cells is highly dependent on actin cytoskeleton. Then, analyzing fluid phase endocytosis of dextrans, we show that constitutive (basal) endocytosis in T-REx293 cells is significantly activated by palmitate/albumin complexes and reduced by inhibitors of palmitoylation, inhibition of the small G protein, RhoA, and by cyclosporines that inhibit mitochondrial PTPs. We go on to show that constitutive endocytosis in T-REx293 cells can be strongly activated by the mitochondrial substrate, pyruvate, in the presence of bicarbonate. It is inhibited by low concentrations of fatty acid-free albumin (15 μM) and can be restored by albumin/palmitate

complexes. While pyruvate is stimulatory, some mitochondrial substrates are inhibitory. Using this model with STED microscopy, we show that vesicles formed via OMDE are 90 to 120 nm in diameter. All results for T-REx293 cells are consistent with mitochondria-dependent OMDE constituting a large fraction of basal PM turnover. However, the constitutive OMDE activity appears to use DHHC acyltransferases besides DHHC5 and DHHC2. In complete contrast to these results, we find that constitutive dextran endocytosis in BMMs is insensitive to all interventions that give positive results for constitutive OMDE in T-REx293 cells. We conclude that constitutive (basal) PM turnover in these different cell types occurs by different mechanisms and that OMDE in BMMs must be activated by cell signaling mechanisms that are not constitutively active in the conditions of these experiments.

Materials and Methods.

Mice. The UT Southwestern Medical Center Animal Care and Use Committee approved all animal studies. The DHHC5 gene-trapped mice were from the same line used previously in which expression of DHHC5 in all tissues tested is reduced by >80% (18, 19). Equal numbers of male and female mice were employed in experiments with no notable significant differences in results.

Primary Cells, Cell Culture and Transfection. *Isolation of Lung Fibroblasts.* Lung fibroblasts of DHHC5-PLM double knock-out animals and their controls were isolated as described elsewhere (20). In brief, animals were euthanized, sterilized with ethanol, and transferred to the laminar flow. Lungs were excised, cut in 1mmx1mm pieces, and placed in a grated Petri-dish. 10 mL of high-glucose DMEM supplemented with 10% heat-inactivated FBS, 50U/mL Penicillin/ and 50µg/mL Streptomycin were added carefully and placed in a humidified incubator with 5% CO_2 at 37°C. After 7-10 days, tissue pieces were removed, and outgrown cells were subjected to experiments after they reached 90% confluency.

Isolation and Differentiation of Bone Marrow Macrophages. Bone marrow cells of DHHC5-PLM double knock-out animals and their controls were isolated as described (21). In brief, animals were euthanized, sterilized with ethanol, and transferred to the laminar flow. Hind limbs were removed, and femur and tibia were cleaned rigorously. Bone marrow was flushed out the bones with 1x PBS and was collected in conical tubes on ice. After resuspension of bone marrow pieces, cells were filtered through a 75 µm cell strainer and the filtered suspension was centrifuged for 5 min at 500xg. The cell number was then determined using a hematocytometer. Cells were seeded at a density of $1x10^6$/six-well well in high-glucose DMEM supplemented with 10% heat-inactivated FBS, 50U/mL Penicillin/ and 50µg/mL Streptomycin and 25 ng/mL M-CSF (PreproTech, Cranbury, NJ). Cells were employed in experiments after 7 days cells. For patch clamp experiments, cells were trypsinized and employed without reattaching to dishes.

Isolation of Peritoneal Macrophages. Peritoneal macrophages of DHHC5 gene trapped mice and their controls were isolated as described previously (22). In brief, animals were euthanized, sterilized with ethanol and the skin layer was carefully removed from the abdomen. The inner skin lining the peritoneal cavity was then carefully punctured and 5 mL of PBS supplemented with 3% FBS were injected. The peritoneal cavity was massaged for about 30 s, the isolation medium was re-aspirated, and cells were transferred to a 50mL conical tube, centrifuged for 5 min at 500xg, resuspended in DMEM supplemented with 10% FBS and thereafter employed in electrophysiological measurements.

Cell Culture and Transfection. T-REx 293 cells were grown in high-glucose DMEM supplemented with 10% heat-inactivated FBS, 50 U/mL Penicillin/ and 50µg/mL Streptomycin in a humidified incubator with 5% CO_2 at 37°C. Transfection of T-REx293 cells with siRNA was performed using Lipofectamine RNAiMAX (Thermo Fisher Scientific, Waltham, MA) according to manufacturer's instructions. siRNAs targeting DHHC 2 and 5 were obtained from Thermo Fisher Scientific (Waltham, MA) and cells were subjected to experiments 48 h after transfection.

Generation of DHHC5/2 knock-out cells. CRISPR knock-out cell lines were produced using established methods (19, 20). The T-REx293 cell line was transiently transfected with LentiCRISPRv2 (Addgene, #52961). The sgRNA sequences used for cloning LentiCRISPRv2-DHHC5 were: DHHC5-forward primer, CCGTGAATAACTGTATTGGTCGC and DHHC5-reverse primer, AAACGCGACCAATACA GTTATTCAC. The sgRNA sequences used for cloning LentiCRISPRv2-DHHC2 were: DHHC2-forward primer, CACCGCGTAGTAGGACCAGCCGAGC and DHHC2-reverse primer, AAACGCTCGGCTGGTCCTACTACGC. The sequencing primer of LentiCRISPRv2 was hU6F: GAGGGCCTATTTCCCATGATT, which was used to verify the sgRNA/Cas9-mediated DHHC2 or DHHC5 gene knockout clones. After the appropriate plasmids were transfected, cells were cultured with medium containing puromycin (10 µg/ml) for one week to select for the surviving cells with the desired plasmids for knockdown of the two genes. For dual knockdown of DHHC2 and DHHC5, cells were co-transfected with LentiCRISPRv2-DHHC5 and LentiCRISPRv2-DHHC2, followed by the relevant selection procedures.

Patch clamp, and capacitance measurement. Axopatch 1C patch clamp amplifiers were employed using our own software for capacitance and conductance recording via square-wave voltage perturbation (23). Unless stated otherwise, solution compositions were the same as employed previously (19). All patch clamp experiments were performed at 0 mV and 35°C. Extracellular solution changes were performed by abruptly moving the microscope stage so as to place the myocyte directly in front of 1 of 4 square pipettes (1 mm) with solution steams maintained by gravity at velocities of 2 to 5 cm/s. In all experiments in which two or more protocols were compared using a single batch of cells, protocols were performed in a randomized fashion.

STED microscopy. STED microscopy was performed in the UTSouthwestern O'Donnell Brain Institute NeuroMicroscopy Core Facility using an Abberior Instruments STED microscope. The Abberior Facility Line system is a 3-D STED super-resolution imaging system. Super-resolution

images were acquired from fixed samples, prepared as described. 30 to 40 nm isotropic resolution was verified in our samples. Adaptive Illumination (RESCue, DyMIN and MINFIELD) was employed with a 60X (NA1.42 WD 0.15mm) Oil Objective. Pulsed 485 nm, 561 nm, and 640 nm lasers were employed. 595 nm and 775 nm STED depletion lasers were employed.

Immunoblotting. For protein isolations cells were washed 3x with pre-cooled PBS and homogenized in pre-cooled RIPA buffer (containing in mM: 150 NaCl, 50 Tris–HCl [pH 8.0], 5 EDTA, 1 EGTA; Triton X-100 1% [vol/vol], deoxycholate 0.5% [wt/vol], SDS 0.1% [wt/vol], and protease inhibitor cocktail from Roche) and lysed for 30 minutes at 4°C. Lysates were cleared at 20,000xg for 15 minutes and subjected to SDS PAGE and subsequent immunoblotting (24). Anti-sera: Anti-ZDHHC5 antibody, produced in rabbit, HPA014670, was from Sigma. Anti-ZDHHC2 antibody, produced in mouse, Clone 1035A (25), was a gift of Dr. Masaki Fukata, Okazaki. Since the DHHC2 antibody provided by Dr. Fukata is no longer available, nor is a comparable antibody available, we subsequently evaluated knockdown of DHHC5 and DHHC2 by qPCR, as described below. Anti-actin was purchased from Santa Cruz (Dallas, TX).

RNA Isolation and Real-Time PCR. RNA isolation and Real-Time PCR were performed as described (26). In brief, total RNA was isolated using Qiagen RNeasy Plus Mini Kits according to manufacturer`s instructions and 1 µg of RNA was reverse transcribed employing the High-Capacity cDNA Reverse Transcription Kit. qPCR was performed on a BioRad (Hercules, CA) CFX96 real time system. Primers for DHHC2 and DHHC5 RNA were as follows: DHHC2 forward primer, TCCCGGTGGTGTTCATCAC. DHHC2-reverse primer, CAACTTGTTCGCCAGTGTTTTC (product length: 99bp). DHHC2-forward primer 2, AACACTGGCGAACAAGTTGTG. DHHC2-reverse primer 2: AGATGGGAAGATCCTTGGCTG (product length: 211bp). DHHC5 forward primer 1, CACCTGCCGCTTTTACCGT. DHHC5-reverse primer 1, CGGCGACCAATACAGTTATTCAC (product length: 111bp). DHHC5-forward primer 2, AACTGTATTGGTCGCCGGAAC. DHHC5 reverse primer 2, AACACACCCATAATGTGGGCT. Knockdowns amounted to 70 and 72% for DHHC2 and DHHC5, respectively.

Acyl-RAC Procedure for Mass Spectrometry. The Acyl-RAC procedure was conducted as described elsewhere (25, 26). In brief, T-REx293 cells were grown to 90% confluency in 10 cm dishes and then subjected to the indicated treatments. The cells were then washed and lysed in 2 mL of lysis buffer (containing in mM: 50 Tris pH 7.2, 5 EDTA, 150 NaCl, 10 NEM, Protease Inhibitor Cocktail (Roche, Basel, Switzerland), 2 PMSF) using Dounce homogenization. Lysates

were then centrifuged at 200,000xg for 30 minutes to separate the membrane and soluble fractions.

Membrane fractions were resuspended in lysis buffer supplemented with 1.7% Triton-X-100 using a 23 G needle. Solutions were then incubated under rotation at 4°C for 1 hour and collected by centrifugation at 250xg for 5 minutes. For acetone precipitation, 3 volumes of ice-cold acetone were added, and the solution was incubated for 30 minutes at -20°C. The solution was then centrifuged at 3000xg for 5 minutes to collect the pellet. The pellets were washed 3 times with pre-cooled 95% ethanol and dried for 5 minutes. The pellet was resuspended in the same volume as before the acetone precipitation in blocking buffer (containing in mM: 20 HEPES pH 7.7, 5 TCEP, 5% [wt/vol] SDS), subjected to BCA, and the concentration was adjusted to 2 mg/mL.

Subsequently, extracts were incubated at 30°C for 30 minutes, 10 mM NEM were added, and extracts were incubated rotating for 1 hour at 37°C. For acetone precipitation, 3 volumes of ice-cold acetone were added, and the solution was incubated overnight at -20°C. The solution was then centrifuged at 3000xg for 5 minutes to collect the pellet. The pellets were washed 3 times with pre-cooled 95% ethanol and dried for 5 minutes. Pellets were resuspended in column buffer (containing in mM: 20 HEPES at pH 7.2, 1 EDTA, 1% [wt/vol] SDS, and the protein concentration was adjusted to 2 mg/mL.

Samples were split in two, and 300 µL of thiol-sepharose slurry washed with column buffer was added to each sample. Corresponding fractions were either treated with a final concentration of 0.7 M freshly prepared hydroxylamine (pH 7.2) or with 0.7 M Tris (pH 7.2). Samples were incubated under rotation overnight (23°C). Beads were allowed to settle by gravity, supernatant was collected, and beads were washed 3 times with 1xPBS. The last wash was removed, 150 µL of 2x TEABC buffer 1 (containing in mM: 50 TEABC) and 25 µg of trypsin/sample were added, and samples were incubated under rotation at 37°C overnight. Beads were allowed to settle by gravity, supernatant was collected, and beads were washed 3 times with 1xPBS. To elute proteins, 150 µL of 2x TEABC buffer 2 was added (50 mM TEABC, 10 mM TCEP), followed by incubation at 37°C for 30 min and collection of supernatants for downstream applications.

Fluid phase dextran uptake assay. T-REx 293 cells were seeded on Matek glass bottom dishes at least 48 h prior to experiments, such that cell confluency was 80-90% at the time of experiments. BMMs were trypsinized on day 6 of differentiation and seeded onto Matek glass bottom dishes for an additional 24 - 48 h. The cells were then washed, pre-treated for 30 minutes

with the saline solution described. For serum/substrate-free experiments, cells were washed 3x in a saline solution containing in mM: 140 NaCl, 5 KCl, 10 HEPES, 0.6 $MgCl_2$, 2 $CaCl_2$, and 0.6 $NaHPO_4$, at pH 7.2. Cells were then incubated for 30 min or 1 h, as indicated, with the same saline solution followed by a chosen treatment, as indicated, before application of the same solution with 100 μM TexasRed lysine-fixable dextran 3000 MW (Thermo Fisher Scientific, Waltham, MA). Uptake times of either 20 or 4 min were employed, as indicated. Thereafter, cells were rapidly placed on ice and rinsed twice with cold solution. In some experiments, cells were stained with WGA 488 for 5 min to visualize the PM, followed by three cold washed. All cells were fixed for 10 minutes with 4% PFA, washed with PBS, stained with Hoechst dye according to the manufacturer's specifications and then overlayed with CitiFluor Mountant AF1 Solution (Electron Microscopy Sciences, Hatfield, PA).

Fluorescence imaging. Imaging at near confocal resolution was carried out with an Aurox Clarity laser-free microscopy system (Abingdon, Oxfordshire, OX14 3DB, UK) (19), employing a Nikon Eclipse TE 2000-S inverted microscope with an APO LWD 40x 1.15 NA water immersion lens. The 50% point spread was 0.7 and 1.6 microns in the lateral and vertical directions, respectively, as determined with a TetraSpeck Fluorescent Microspheres Size Kit (Invitrogen). This compares to 0.6 and 2.9 microns for a 40x 0.95 NA air lens employed on a standard spinning disc microscope (Nikon CSU-W1 spinning disk with Hamamatsu Orca Fusion camera, Nikon CSU-W1 SoRa: Quantitative Light Microscopy Core Facility, UTSouthwestern). Equivalent images obtained from the same slide (FluoCells prepared slide #3, Invitrogen) with these two imaging systems were provided previously (27).

Analysis of dextran uptake assays. All bar graphs depicting dextran uptake correspond to the analysis of 12 or more fields of view from at least two dishes of cells fixed as described. Fig. 2 illustrates our routine analysis of the dextran uptake assays using a relatively complex sample in which cell density reached confluence in some regions and was sparse in others. Figs.2A to 1C show the fluorescent dextran and Hoechst dye images of a field of T-REx293 cells (~150 cells) that was treated and fixed as described above. Using ImageJ software, a threshold fluorescence was set high enough to eliminate background fluorescence in cells fixed without dextran (not shown). Particles were then identified and outlined, as shown in Fig. 2C using an upper limit set to 2 square microns. Particles were counted in this without setting a lower particle size limit, the influence of which is described subsequently. The number of nuclei were determined as described in Figs. 2C and 1D. As apparent

in the Hoechst image in Fig. 2C, nuclei often overlapped in regions where the cell culture was nearly confluent. As shown in Fig. 2C, the ImageJ software was then unable to accurately separate nucleus images, so that automated nucleus counting became impossible. Therefore, we used two other strategies to determine the number of nuclei. In some cases, we counted nuclei manually after marking them individually via ImageJ. Second, we determined the total nuclear area, as defined by nuclei outlines as in Fig. 2D, and then divided the total area by the average nucleus area determined from 20 to 40 individual nucleus area measurements. As indicated below Fig. 2D, the two approaches yielded values that did not differ by more than 5 to 6%, 153 and 144 nuclei in this case.

Figures 2E to 2G illustrate the analysis of dextran uptake using different criteria. The data shown are from the experiment described subsequently in Fig. 8B, demonstrating that dextran uptake is markedly inhibited by fatty acid free albumin (15 μM) but not by 2:1 palmitate/albumin complexes at the same concentration. Figs. 2E and 2F show results as a particles per cell for the three conditions without setting a lower particle size threshold and after setting a lower particle size limit to 0.25 square microns (i.e. a diameter of 500 nm). In the latter case, the number of apparent particles is 5-times less and the apparent dextran uptake is reduced by only 405 versus 60%. Based on our subsequent analysis using STED microscopy, we conclude empirically that the former analysis (Fig. 2E), generating much higher particle numbers, is likely to be more accurate. This can be justified by the fact that the threshold method employed results distorts the dimensions of many particles to be smaller than the wavelength of light. Finally, Fig. 2G shows the same experimental results quantified as total particle area per total nuclear area, instead of particles per cell. The results are quantitatively very similar to results for particle numbers, indicating simply that average particle size is not changing with albumin treatments.

Chemicals. Unless stated otherwise, chemicals were from Sigma-Millipore (St. Louis, MO) and were the highest grade available.

Experimental Design and Statistics. All patch clamp results presented were similar in sets of experiments performed on at least 3 different days. When practical, experiments were performed in a blinded or double-blinded fashion. In each uptake assay, at least two dishes of cells were analyzed for each experimental condition, and similar results were obtained in at least two different sets of experiments. All bar graphs depicting dextran uptake include at least 12 images from two dishes of cells. Significance of results was determined via Students' t-test, except in rare cases when results were not normally distributed. In those cases, significance was determined by Mann-Whitney Rank Sum test. Error bars represent Standard Error.

Results.

DHHC5/2-dependent OMDE: Activation by GTPγS and oxidative metabolism in patch clamped T-REx293 cells and BMMs. Figure 3 describes large-scale OMDE that can be activated without Ca elevations in T-REx293 cells and BMMs. Fig. 3A presents representative capacitance and conductance records from a T-REx293 cell that was opened via patch clamp with a pipette solution containing GTPγS (0.2 mM), MgATP (10 mM) and EGTA (10 mM) with no added Ca. Free cytoplasmic Ca is thus essentially zero. After opening the cell by suction, the cell was moved quickly into a solution stream that is warmed to 35°C. Without any discernable changes of cell conductance, membrane capacitance (i.e. PM area) decreases by about 40% over 8 min. As described previously (28), this response is accelerated several fold, and enhanced, when T-REx293 cells overexpress the cardiac NCX1 Na/Ca exchanger, which is palmitoylated at one cysteine close to the PM (28). Fig. 3B illustrates additional key features of OMDE activated by GTPγS, not described previously. From left to right, the response in cells without NCX1 expression amounts on average to a 40% loss of PM over 8 min. Using T-TEx293 cells in which two DHHCs, known to reach the PM, DHHC5 and DHHC2 (29-31), are knocked out by CSPR (see Supplemental Fig. S2), the PM loss is decreased to 18%. Cytoplasmic carnitine is a substrate of carnitine palmitoyl transferase, which converts long-chain acyl-CoAs to acylcarnitines that are transported into mitochondria and resynthesized to acyl-CoAs (32). The endocytic response is decreased to less than 5% when 5 mM carnitine is included in the pipette solution, presumably by depleting the cytoplasmic pool of long-chain acyl-CoAs. If correct, this would mean that long-chain acyl-CoAs are limiting for the endocytic response under the conditions of these experiments. When actin cytoskeleton is disrupted by treating cells for 10 min with latrunculin (0.5 μM), and including latruculin (2 μM) in the pipette, the PM loss is not only inhibited, it is replaced by a PM expansion response of about 25%. Nevertheless, the loss of PM induced by GTPγS can be fully restored by performing the same experiments with a 30% hypotonic solution to induce cell shrinkage or by simply applying enough suction to the pipette tip to cause a detectable amount of cell shrinkage. From these results, we suggest that latrunculin may inhibit endocytosis by allowing the PM to expand and stretch, thereby generating a lateral membrane tension that hinders membrane budding. This interpretation is essentially the same as proposed for actin engagement in clathrin-mediated endoctyosis (33). Further, however, these results suggest that G-proteins activated by GTPγS must promote endocytosis by mechanisms besides the modulation of membrane actin cytoskeleton.

Figure 3C illustrates two manipulations of mitochondrial metabolism that are key to our subsequent analysis of OMDE in T-REx293 cells in culture. When cells are opened in the presence of GTP (0.3 mM), MgATP (10 mM) and minimal Ca buffering (0.5 mM EGTA with 0.25 mM Ca, giving about 0.25

μM free Ca), PM loss amounts to about 17% over 8 min. This loss is decreased by 60% when the mitochondrial substrate, β-hydroxybutyrate (β-HB, 10 mM) is included in the pipette, but the loss is enhanced 2.5-fold when the same concentration of the mitochondrial substrate, pyruvate, is included in the pipette. Evidently, therefore, the metabolism of mitochondrial substrates is a major determinant of OMDE, and the extent to which ROS are formed during their metabolism is one potentially important determinant of OMDE progression.

Figures 3D and 3E illustrate the exceptionally powerful OMDE activity of murine BMMs, differentiated for 7 days by hematopoietic growth factor, M-CSF(34). We note that capacitance measurements (not shown) revealed that BMMs develop about 10 times more PM during differentiation. As shown in Fig. 3D, upon PM *opening* by patch clamp with pipettes containing succinate (8 mM), cells take in >75% of their PM within 2.5 min. These massive OMDE responses are characterized in detail in Fig. 3E. From left to right, PM loss amounts to only about 10% of the PM when mitochondrial substrates are not included in the pipette, in spite of the fact that the cytoplasm contains 10 mM ATP (and 0.2 mM GTP). The OMDE responses are decreased by 65% in BMMs from DHHC5-gene-trapped (GT) mice, inhibited >80% by the mitochondria-selective cyclosporine, NIM811 (a blocker of PTPs, (35)), and inhibited 65% by 2:1 bromopalmitate/albumin complexes (160/80 μM). The OMDE responses are inhibited similarly when the antioxidant, tiron (36), is included in the pipette at a high concentration (15 mM), and the responses are inhibited about 70% by when cells are pretreated for 10 min with latrunculin (0.5 μM). OMDE responses are effectively absent when β-HB (15 mM) is used as the mitochondrial substrate, potentially because β-HB has antioxidant activity at or in mitochondrial membranes (37). In complete contrast to β-HB, pyruvate (15 mM) supports OMDE responses that are equally large as succinate responses. Shown as a red bar graph, endocytic response of BMMs induced by including GTPγS (0.3 mM) in the pipette are also fully equivalent to the succinate responses, even in the presence of 10 mM EGTA with no added Ca. Finally, shown in blue, equivalent OMDE responses are activated by 90 μM Triton-X100 without Ca or substrates, presumably because nonionic detergents at low concentration induce membrane phase separations in complex membranes (12, 38).

Results shown in Fig. 4 verify in two further cell types that OMDE responses induced by succinate are dependent on DHHC acyltransferase activity. Using murine lung fibroblasts and acutely isolated peritoneal macrophages from WT mice, OMDE responses in the presence of succinate amounted to 48% and 46% of total PM, respectively. In the former case, responses were reduced to 23% in cells from DHHC5 gene-trapped animals, and in the latter case the endocytic responses were converted to membrane expansion in cells from the gene-trapped animals. In summary, OMDE in macrophages

and fibroblasts is very powerful when activated by GTPγS or mitochondrial metabolism of succinate or pyruvate. The endocytic responses are far too large to be accounted for by caveolae (10) and are larger than any descriptions of clathrin/dynamin-dependent endocytosis known to us.

OMDE is constitutively active in T-REx293 cells but not dependent on DHHC5 or DHHC2. Figure 5 shows initial evidence that OMDE is constitutively active in T-REx293 cells. As described in Methods, cells were incubated in a simple physiological saline solution without serum or substrates for 1 h. Thereafter, cells were incubated with 3 kD TexaRed™- lysine-fixable-dextran for 20 min, the PM was labeled with wheat germ agglutinin (WGA) on ice, cells were fixed for 10 min with 4% paraformaldehyde, and nuclei were labeled with Hoechst dye (not shown). Fig. 5A is a typical micrograph of a control cell, showing the overlayed fluorescence of dextran (red) and WGA (green). Fig. 5B shows the time course of dextran uptake, determined in duplicate measurements at the time points indicated after initiating uptake. Dextran uptake saturates within about 10 min, and the apparent time constant is 7.4 min.

That OMDE may be an important mechanism of constitutive PM turnover in T-REx293 cells is supported by the following results (Figs. 5C-5E). Inhibition and stimulation of uptake by bromopalmitate/albumin and palmitate/albumin complexes are shown in Fig. 5C. We note that we employed albumin complexes of both compounds to avoid nonspecific membrane effects and because albumin effectively delivers these compounds into cells via fatty acid transporters (39). Control uptake (blue) was determined in the presence of 0.1 mM fatty acid-free albumin. Then, in the presence of 3:1 bromopalmitate/albumin complexes (0.3/0.1 mM), which inhibit DHHCs (40), uptake is decreased by ~70%. In contrast, uptake is increased by 40% in the presence of equivalent palmitate/albumin complexes. As shown in Fig. 5D, dextran uptake is inhibited 60% by 1 μM cyclosporine A (CsA), an inhibitor of PTP openings (41) that can block OMDE (42). Subsequent results illustrate inhibition of dextran uptake by metabolites that may shift long-chain acyl-CoA into mitochondria or shift CoA from long-chain acyl-CoA to other CoA activated metabolites. Specifically, uptake is decreased significantly in cells incubated for 10 min with carnitine (10 mM) and with butyrate (10 mM). Fig. 5E shows that dextran uptake is decreased by a newly identified DHHC inhibitor (43) (PATi, 10 μM) and is also significantly decreased by RhoA inhibition with C3-transferase (Rho Inhibitor I, (44)). We mention in this connection that RhoA has recently been shown to activate endocytosis that promotes migration of macrophages in an amoeboidal migration mode (45).

Finally, Fig. 5F presents the results of DHHC5 and DHHC2 knockdown experiments using siRNAs, as described in Methods. Verified oligonucleotide sequences were employed to knock down DHHC5 and DHHC2 via transfection with Lipofectamine RNAiMAX. Knockdown was verified by Western

blotting and qPCR for DHHC5. Knockdown of DHHC2 was verified by qPCR. As apparent in Fig. 5F, neither the knockdown of DHHC5, nor DHHC2, nor knockdown of both DHHCs significantly changed the constitutive uptake of dextran by T-REx293 cells. We conclude therefore that these DHHCs are not essential for constitutive PM turnover in these cells. Other acyltransferases must be involved, if palmitoylation of PM proteins is indeed importantly involved in constitutive endocytosis in the absence of serum and mitochondrial substrates.

Activation of dextran uptake by mitochondrial substrates and bicarbonate. Relevant to patch clamp studies in Figs. 3 and 4, we next tested if (and when) mitochondrial substrates might significantly affect dextran uptake in T-REx293 cells. To do so, we first included the mitochondrial substrate, acetate, in the saline solution employed, and we subsequently included bicarbonate (25 mM, at pH 7.2) to support cell carboxylase activities that might be important for the effects of mitochondrial substrates. Fig. 6 shows the major results. From left to right, Fig. 6A shows that cyclosporin A (1 μM) has a particularly strong inhibitory effect on dextran uptake in the presence of acetate. Carnitine (10 mM) is mildly inhibitory (Fig. 6B) when compared to patch clamp results. Pyruvate (10 mM) is inhibitory in the presence of acetate and absence of bicarbonate (Fig. 6C), and β-HB (10 mM) is strongly inhibitory, similar to cyclosporin A. In Supplementary Fig. S3 we verify that metabolic substrates, specifically pyruvate and β-HB (which generate metabolites activated by CoA), can indeed reduce total long-chain acyl-CoAs by 30 to 50% in HEK293 cells. We show further that carnitine significantly increases long-chain acyl-CoAs, presumably related to a shifting of acyl groups into mitochondria. Finally, in Fig. 6C, we shown that cyclosporin A (1 μM) is also inhibitory in the presence of pyruvate.

A major enigma raised by these results is why pyruvate is inhibitory in cultured cells but is strongly stimulatory in patch clamp studies. One possible explanation is that pyruvate rapidly reaches the same cytoplasmic concentration as the concentration included in the pipette during patch clamp experiments. In contrast, the cytoplasmic pyruvate concentration likely remains only a small fraction of the extracellular concentration in experiments in intact cells, and the generation of citric acid cycle metabolites from pyruvate may be limited by pyruvate metabolism. One potential limitation, therefore, may be the lack of bicarbonate in these experiments, which would limit pyruvate entry into mitochondrial metabolism via pyruvate carboxylation to oxaloacetate (versus pyruvate decarboxylation to acetyl-CoA). As shown in Fig. 6D and Fig. 7, the inclusion of bicarbonate (25 mM) in the saline solution employed resulted in a large and reliable stimulation of dextran uptake by pyruvate. As shown in Fig. 7, the stimulatory effect sometimes reached a tripling of dextran uptake.

Pyruvate stimulation of dextran endocytosis is inhibited by β-HB and bromopalmitate/albumin complexes. In patch clamp studies, pyruvate and β-HB usually have opposite (antagonistic) effects on endocytosis (Fig. 3). Therefore, we compared their effects and interactions in dextran uptake experiments in the presence of acetate and bicarbonate. As shown in Fig. 7, β-HB (12 mM) reduced dextran uptake by just 50%. Note that in this experimental set pyruvate (12 mM) increased dextran uptake by 2.5 fold. In the presence of β-HB (12 mM), pyruvate (12 mM) increased uptake only to the baseline uptake. In other words, β-HB effectively blocks the stimulatory effect of pyruvate on endocytosis. The inhibitory effects of β-HB are in fact even stronger than those of bromopalmitate/albumin complexes (0.2/0.1 mM), shown in Fig. 7B. While BP complexes inhibit basal dextran uptake similarly to β-HB, about 50%, pyruvate still increases dextran uptake in the presence of BP to a level that is somewhat greater than control uptake. We conclude that β-HB must be acting with some specificity to block the signaling mechanisms that pyruvate activates to stimulate constitutive PM turnover. As already noted, an antioxidant activity of ketone bodies near or within mitochondrial membranes is one possible simple explanation (46).

Given that the effects of pyruvate to stimulate OMDE may involve ROS and the opening of PTPs to release CoA, the question is raised whether these mechanisms might cause cells to undergo apoptosis. To test this, we subjected dishes of cells to the protocols that induce endocytosis by pyruvate and then returned the cells to normal culture conditions (i.e with high glucose DMEM medium and 10% serum). After 24 h, we stained cells with trypan blue to test for the presence of dying or dead cells. As illustrated in Supplemental Fig. 4, we found no evidence for damaged or apoptotic cells in cultures that were treated with the pyruvate protocol.

Fatty acid-free albumin inhibits dextran uptake at low micromolar concentrations. In our early patch clamp experiments on endocytosis in BHK cells (42), we found that OMDE was inhibited by treating cells with fatty acid free albumin, and that OMDE could be restored by restoring fatty acids that had evidently been extracted from cells by albumin. Accordingly, we tested to what extent fatty acid free albumin might inhibit constitutive endocytosis in T-REx293 cells. To our surprise, we found that albumin was effective at low micromolar concentrations. Fig. 8 shows results for treatment of cells with albumin (15 μM) prior to, but not including, the uptake measurement (8A), as well as for continuous treatment including the dextran incubation period (8B). The exact protocols employed are illustrated above the bar graphs in each panel. For results in Fig. 8A, one group of cells was incubated with acetate/bicarbonate-containing saline for 60 min, and then with dextran for 4 min ("1."). In a second group, saline was administered for 30 min followed by saline with 15 μM albumin for 30 min, and finally with dextran and no albumin for 4 min ("2"). In a third group, albumin (15 μM) was loaded

with palmitate (30 μM) at a 2:1 ratio was applied for 30 min followed by dextran without albumin ("3"). Pretreatment with albumin reduced dextran uptake by 57%, whereas uptake was reduced only 38% for albumin loaded with palmitate. Fig. 8B shows the equivalent results when albumin was administered for 10 min followed by dextran for 10 min with albumin or albumin with palmitate. In this protocol, the dextran uptake is reduced 40% by albumin, and the presence of palmitate entirely precludes the effect of albumin. As described next, it appears that FA-free albumin indeed can decrease palmitoylations of PM proteins that may be involved in endocytosis, and effect that would appear to require PM-localized acyl-CoA turnover that in turn depends on local FA concentrations.

Inhibition of PM palmitoylations by carnitine, β-HB and FA-free albumin. Next, we tested whether key protocols that inhibit endocytosis (which might depend on reducing palmitoylations) actually do inhibit palmitoylations of PM proteins. To do so we incubated 10 cm dishes of T-REx293 cells equivalently to the protocols employed for uptake assays. Cells were incubated with the saline solution containing acetate and bicarbonate for 1 h. Thereafter, cells were incubated with either 10 mM carnitine + 10 mM β-HB or with 15 μM FA-free albumin for 30 min. Cells were then harvested as described in Methods to isolate membranes, followed by blockade of free cysteines, deacylation with hydroxylamine and pull-down of palmitoylated proteins via the acyl-RAC method (47). Selected results from the proteomic analysis by mass spectrometry are shown in Fig. 9A. In brief, the palmitoylation of many PM proteins, confirmed multiple times in the SwissPalm palmitoylation database (https://swisspalm.org), are decreased. We point out in this regard that the acyl-RAC method identifies only proteins that are completely depalmitoylated -- proteins that are palmitoylated multiple sites are often not identified. The 17 proteins listed were highly enriched by the hydroxylamine treatment (see enrichment values in parentheses). Carnitine/β-HB treatment for 30 min or incubation with low concentrations of FA-free albumin for 30 min strongly decreased the pull-down of many of these proteins. Those that do not change (caveolin-1, flotillins, and VAMP-3) may have long-lived acylations ***or*** be palmitoylated by DHHCs with very high affinity for acyl-CoAs. The identification of multiple Annexin proteins in this assay may be relevant to OMDE activation by Ca (48), and the cytoskeleton- associated proteins identified, including vimentin and α-actinin, may be relevant to the actin-dependence of OMDE.

Reciprocal effects of palmitoylation on uptake of cholera toxin B (CTB) and transferrin (TF). Knowing that multiple biologic interventions that inhibit OMDE also appear to inhibit palmitoylations of multiple PM proteins, we next examined the effects of one of those treatments (carnitine+β-HB) on endocytosis defined by two classical membrane markers, CTB and TF. While neither of these probes is entirely specific, CTB binds selectively GM1 gangliosides and is internalized primarily by

clathrin/dynamin-independent mechanisms. We note however that CTB is also taken up to some extent by clathrin endocytosis (49, 50) in addition to 'raft' endocytosis. TF, on the other hand, is internalized primarily by classical clathrin-dependent endocytosis (51). Using a 2 min uptake assay under substrate- and serum-free conditions to define constitutive uptake, the uptake magnitudes were similar for the two probes (see micrographs in Figs. 9B and C, and composite results in Figs. 9D and 9E). Nevertheless, uptake of CTB was decreased ~40% by the carnitine/β-HB treatment ($p<0.01$) while TF uptake was significantly increased ($p<0.01$). Regarding the increase of TF uptake, it was described already in 1990 that transferrin palmitoylation hinders clathrin endocytosis and that depalmitoylation promotes iron uptake (52). Overall, these results verify the major two pathways of endocytosis, as we prefer to define them, are affected differently by interventions that likley affect formation of ordered membrane domains. The results are consistent with OMDE mediating much of the CTB uptake in T-REx293 cells. While OMDE contributes to basal PM turnover in T-REx293 cells, a substantial contribution of clathrin endocytosis is also indicated.

STED microscopy reveals dimensions of endocytic vesicles formed by constitutive OMDE.

To address the membrane structures formed during OMDE, we initiated super-resolution optical studies with STED microscopy (53). Using 10 kD CF640R-dextran to monitor fluid phase endocytosis, Fig. 10A shows a representative micrograph for 2 min dextran uptake in T-REx293 cells. Within the 2 min, 514 puncta form with diameters described in histograms in Figs. 10B and 10C. Converting the surface areas of particles to spherical areas, the uptake constitutes a loss of ~110 μm^2 of PM. This corresponds to ~1 pF or ~1% of the PM of a large T-REx293 cell. The histograms of puncta diameters appear to have two components in control cells (Fig. 10B). To acutely inhibit OMDE, we treated cells as above with carnitine (5 mM) and β-HB (5 mM). The histogram from treated cells, shown in Fig. 10C, is paired experimentally with the control histogram in Fig.10 B. Treatment to decrease palmitoylations results in a decrease of average vesicle size from114 to 95 μm., and a decrease of mean vesicle size from 94 to 71 nm ($p<0.001$). Cell morphology was stable, and the number of particles in the size range from 85 to 130 nm was significantly decreased. Assuming that OMDE is primarily blocked in these experiments, rather than clathrin endocytosis, we conclude that the vesicles formed by OMDE are on average larger than vesicles formed by clathrin endocytosis but very substantially smaller than vesicles formed by macropinocytosis (54).

Mitochondria-dependent OMDE does not contribute to constitutive endocytosis in BMMs.

Finally, Fig. 11 presents our analysis of constitutive endocytosis in BBMs, i.e. in the absence of serum and mitochondrial substrates, indicating that OMDE is inactive in the basal state of these cells. Fig.

11A is an overlay from a representative assay of nucleus outlines and particle outlines in an Aurox field of view. There are 120 nuclei and on average 30 particles per cell, about 3-fold fewer particles per cell than found in T-REx293 cells under these conditions and using identical analysis parameters. As shown in Fig. 11B, bromopalmitate/albumin complexes (0.3/0.1 mM) have no effect on dextran uptake in experiments carried out identically to those for T-REx293 cells in Fig. 5. Palmitate/albumin complexes (0.3/01 mM) increase uptake only marginally. Fig. 11C shows that cyclosporin A (2 μM) is without significant effect on uptake, and Fig. 11D illustrates the insensitivity of uptake to addition of β-HB (10 mM) and pyruvate (10 mM). Finally, as shown in Fig. 10E, dextran uptake was unchanged in these conditions in BMM cultures from mice lacking DHHC5. From these results, we conclude that the massive endocytic mechanisms described in patch clamp experiments with BMMs (Fig. 3), employing high concentrations of mitochondrial substrates or GTPγS (Fig. 3B), are effectively inactive in the absence of serum and metabolic substrates (i.e. in the basal/constitutive state of these cells).

Discussion.

In this article we have verified that three forms of "activated" OMDE are supported by and/or require the acyltransferases, DHHC5 and DHHC2. We have compared constitutive endocytosis in T-REx293 cells and murine BMMs with fundamentally different outcomes. In the absence of serum and mitochondrial substrates, T-REx293 cells have a large endocytic flux that is consistent with OMDE under mitochondrial control, while equivalent experiments in BMMs are entirely negative. In contrast to OMDE activated in patch clamp experiments, we find no involvement of DHHC5 or DHHC2 acyltransferases in constitutive OMDE in T-REx293 cells. We have described that small metabolites, namely pyruvate and β-HA, can markedly modify OMDE, and that classical clathrin endocytosis is likely affected in a reciprocal manner. Remarkably low FA-free albumin concentrations can inhibit constitutive OMDE in parallel with an apparent decrease of PM protein palmitoylations. Finally, we have analyzed the physical basis of constitutive OMDE via STED microscopy in T-REx293 cells. Endocytic vesicles formed during constitutive OMDE have diameters of 90 to roughly 140 microns, distinctly larger than average vesicles formed via coated pits (i.e. clathrin endocytosis) but substantially smaller than vesicles formed by macropinocytosis (54). We discuss these Results roughly in the order of their presentation.

OMDE activated by G-proteins and oxidative metabolism in T-REx293 cells and BBMs.

We have documented in Figs. 3 and 4 the extraordinary power of OMDE when activated by cytoplasmic GTPγS or mitochondrial substrates in T-REx293 cells and murine BBMs. The occurrence of massive endocytosis in the presence of a high (0.2 mM) concentration of GTYγS, which cannot be hydrolyzed by dynamins, makes the involvement of dynamin GTPase very unlikely (48). While we have not defined which G-proteins can be involved, we point out that the involvement of multiple small G-proteins in clathrin/dynamin-independent endocytosis has been well established for decades (55). Inhibition of the RhoA is clearly inhibitory (Fig. 5E). We demonstrate in Fig. 2 that OMDE activated in both T-Rex293 cells and BMMs is dependent on DHHC acyl-transfer activities, as well as actin cytoskeleton. In the case of T-REx293 cells we have used siRNA of two DHHC enzymes, known to reach the PM, DHHC5 (31) and DHHC2 (30), to demonstrate dependence of GTPγS-activated OMDE on acyltransferase activity. In the case of cultured BMMs, we have employed cells from DHHC5 gene-trapped animals (18) to demonstrate dependence of succinate-activated OMDE on acyltransferase activity. For lung fibroblasts and acutely isolated peritoneal macrophages, we have demonstrated a dependence of succinate activated OMDE on DHHC5 using cells from the gene-trapped animals (Fig. 3A).

Concerning actin-dependence, endocytosis induced both by GTPγS and by succinate metabolism is decreased more than 60% by latrunculin (Figs. 3B and 3E). This contrasts to our previous studies of massive endocytosis induced by Ca elevations in which latrunculin was without effect (48, 56) The obvious difference between the different forms of OMDE is that Ca initially causes a large membrane expansion that may release PM tension (48). Consistent with this interpretation, the block of OMDE in T-REx293 cells by latrunculin can be fully overcome by cell shrinkage, employing hypotonic cytoplasmic solutions or by applying negative pressure to the pipette (Fig. 3B). Both of these interventions are expected to decrease lateral membrane tension, and it is now essential to test whether inhibitory effects of actin disruption on 'bulk endocytosis' in neurons (57) is also dependent on lateral PM tension.

We have suggested previously that ROS generation by mitochondria is a major signaling factor that promotes massive endocytosis via OMDE (42). ROS may act through many signaling mechanisms, including the activation of small G-proteins (58), but in addition our work suggests that the opening of mitochondrial PTPs (permeability transition pores) is critical, namely to release mitochondrial metabolites, in particular CoA, to the cytoplasm (42). These suggestions are supported in the present study by the effective block of succinate-activated OMDE in BMMs by the mitochondria-specific cyclosporin, NIM811, and by the antioxidant, tiron (Fig. 3). Admittedly, tiron is not a specific antioxidant, as it chelates iron as well as other multivalent metals (36). We point out in this connection that attempts to block PTP openings with antioxidants have often had mixed or complex outcomes (e.g. (59, 60)). In-so-far as OMDE depends on PTP openings that are activated by oxidation of cysteines, the consistently small magnitude of OMDE that occurs with β-HB, and the ability of β-HB to suppress pyruvate activation of OMDE (Fig. 7A), may be relevant to beneficial effects of β-HB found in several degenerative disease models (e.g. (61)). That fact that cytoplasmic pyruvate, like succinate, strongly activates OMDE in both T-Rex293 cells and in BBMs was surprising, since the cytoplasmic metabolism of pyruvate has antioxidant functions (e.g.(62)). In the simplest case, β-HB may function as a membrane-near antioxidant at critical mitochondrial sites, presumably adjacent to cytochrome oxidases where local ROS generation promotes PTP openings.

The speed and magnitude of OMDE activated by succinate and pyruvate in BBMs (Fig. 3) are unprecedented for any form of biological endocytosis known to us. On average 77% of the PM is removed within 2 to 3 minutes. Since these responses can occur even when cytoplasmic Ca is heavily buffered (10 mM EGTA with 3 mM Ca (Fig. 3B)), Ca elevations are definitively not required. As already pointed out, the generation of ROS and PTP openings are both implicated for succinate-induced OMDE. The fact that endocytic responses to pipette perfusion of GTPγS are very similar in

magnitude (and speed) indicates that G-proteins besides dynamins are very likely involved. Induction of similar endocytic responses by low concentrations of TritonX-100 is consistent with our hypothesis that growth of ordered domains drives these endocytic responses. Nonionic detergents are long known to cause phase separations of complex membranes at low concentrations (see (38)). We hypothesized therefore that in the PM of most cells, the phase separation of lipids additionally brings involvement of PM proteins that can accumulate in ordered membrane domains. By involving PM proteins, in particular palmitoylated proteins, OMDE can internalize far larger fractions of the PM than would be expected from the presence of so-called lipid rafts, which in general are expected to make up only a small fraction of the plasma membrane (63).

The constitutive roles and regulation of PTPs.

While it is established beyond reasonable doubt that mitochondrial PTP openings are associated with mitochondrial depolarizations and eventually the initiation of cell death programs (64), the physical identity of PTPs and their signaling roles in normal cell physiology remain controversial (65, 66). That PTPs can open transiently in a so-called 'flickering', low conductance mode during normal cell physiology is definitively established, and such openings are in general thought to release calcium from mitochondria and to mediate 'flashes' of mitochondrial ROS. Our hypothesis, however, that PTPs can release significant amount of coenzyme A physiologically requires that physiological PTP openings generate significant mitochondrial permeability to relatively large solutes. In fact, studies employing calcein release to monitor PTP openings do indeed document significant solute release in a spontaneous and maintained fashion from individual mitochondria (67, 68), and such openings have been implicated to regulate some forms of cell reprogramming (69). Furthermore, solute release associated with electrical spiking is documented to occur in bacteria (70) and may be an evolutionarily early form of cell signaling (e.g. (71)). A strong limitation of our work on OMDE up to now has been the fact that most experiments involved patch clamp, an experimental model that does not readily allow biochemical experimentation. The strong inhibitory effect of cyclosporin A on dextran uptake in cells cultured in the presence of bicarbonate (Fig. 6) now provides an experimental model to test in detail whether the generation of long-chain acyl-CoAs and cysteine palmitoylations are modified in parallel with OMDE.

Constitutive activity of OMDE is highly variable between cell types.

Often, attempts to define specific endocytic mechanisms and their involvement in PM turnover employ molecular biological means to overexpress or to delete individual endocytic proteins. The caveat then is that cells may adapt and compensate genetic interventions in the time frame required to

induce protein changes. We elected therefore, for the limited purposes of this article, to examine acute interventions that with modest confidence can indicate which mechanisms are active. To test whether OMDE under mitochondrial control is constitutively active in T-REx293 cells, we initially cultured cells without serum or metabolic substrates for 1 h in a simple physiological saline solution. In this substrate-poor environment (Fig. 3), we found that PM turnover was strongly decreased by bromopalmitate/albumin complexes and could be increased by albumin/palmitate complexes. These results are non-specific but are consistent with palmitoylations of PM proteins being required for basal PM turnover. PM turnover was decreased by >50% by a cyclosporin (cyclosporin A) that suppresses PTP openings. This specific result is nonspecific because cyclosporin A is also an inhibitor of the phosphatase, calcineurin. However, we showed previously and in the present study that the mitochondria-specific cyclosporin, NIM811, is very effective. Basal PM turnover was decreased by a recently developed DHHC inhibitor, PATi (43), consistent with DHHC involvement. Basal PM turnover was significantly decreased by carnitine, which can be expected to shift cytosolic acyl-CoA into mitochondria via the intermediate, acyl-carnitine. Basal PM turnover was inhibited significantly by inhibition of the small G-protein, RhoA. consistent with evidence that multiple forms of OMDE are dependent on small G protein actively. Subsequently, in the presence of a mitochondrial substrate, acetate (10 mM), we found that constitutive endocytosis was decreased strongly by cyclosporin A, inhibited significantly by carnitine, inhibited significantly by pyruvate (10 mM) and inhibited strongly by hydroxybutyrate. These latter results are at least consistent the idea that small metabolites that are activated by CoA can decrease long-chain acyl CoAs by shifting CoA to other metabolites. Importantly, we have verified that these same metabolites can indeed decrease long-chain acyl CoAs under the conditions of these experiments. These results together are at minimum supportive of a significant role of OMDE under mitochondrial control contributing to constitutive PM turnover in T-REx293 cells. This impression is then strengthened very strongly by the fact that constitutive PM turnover in differentiated BMMs is not sensitive to this same group of acute interventions, even though OMDE, when activated can be much more powerful in BMMs than in T-REx293 cells.

As noted in the Introduction, the present study was initiated in response to an article suggesting that constitutive PM turnover in HeLa cells occurs exclusively via conventional clathrin/dynamin-dependent endocytosis (9). This conclusion was surprising as we had shown previously that OMDE in BHK cells, when activated by Ca elevations, can be nearly 100 times more rapid than the measured rates of basal PM turnover in BHK cells. Thus, it seemed readily possible that OMDE could be a major component of constitutive PM turnover. The clear outcome of the present study is that OMDE may or may not play significant roles in basal PM turnover. In strong contrast to results for T-REx293 cells, experiments using BMMs do not suggest any role of OMDE under mitochondrial control in basal

PM turnover (Fig. 11), defined as being PM turnover that occurs without serum or external metabolic substrates. This outcome seem especially notable because OMDE in BMMs, when activated, can be substantially larger and faster than OMDE in T-REx293 cells. We conclude that the role of OMDE in constitutive PM turnover is highly variable and very probably depends on the detailed functional state of cells in culture. It is also notable in this connection that, although constitutive endocytosis in T-REx293 cells appears to be dependent on fatty acids and eventually palmitoylations, it is not dependent on the presence of the DHHC2 or DHHC5 acyltransferases (Fig. 5F). Given that cells contain more than 20 DHHC isoforms (72), it does not seem surprising that different DHHC enzymes are critical in different cell conditions. Assuming that coenzyme A and long-chain acyl-CoAs are relatively low in the conditions of these measurements, DHHC enzymes with relatively high affinities for substrates might be required.

The physical and biochemical basis of OMDE and its modulation by albumin.

As noted in the Introduction and documented in Results, OMDE clearly involves the ordering of both lipids and membrane proteins into domains and can also involve the actin cytoskeleton. It also seems likely that the presence of different protein cargos initiates OMDE with different physical characteristic. In the form of OMDE dubbed 'CLIC', for example, the palmitoylated 'raft' protein, CD44, is a major cargo, and endocytic vesicles take on a tubular form that may be determined both by CD44 and the branching of actin cytoskeleton that appears to contribute to the endocytic process (14, 73). Up to now, visualizing endocytic structures with STED microscopy, we have not clearly observed tubular structures. Accordingly, it will be important to test whether the overexpression of different cargo proteins may dictate how OMDE develops and which structural features can be influenced by the expression of different cargos.

The work presented in this article provides a new basis to analyze OMDE using coordinated patch clamp and cell culture/biochemical approaches. The most surprising result, which requires experimental attention, is that low FA-free albumin concentrations substantially decrease OMDE in parallel with a decrease PM protein palmitoylations. Two drastically different interpretations of these results are presently possible. On the one hand, albumin is known to directly interact with membranes, in particular cholesterol-rich membranes (e.g. (74)). Thus, FA-free albumin might induce changes of membrane structure (and possibly PM ordering) that either inhibit the palmitoylation of PM protein or promote the depalmitoylation of PM proteins. On the other hand, the extraction of FAs from the PM by albumin might decrease the availability of FAs on the cytoplasmic side for activation by acyl-CoA synthetase(s) associated with the PM and their subsequent use by DHHCs to palmitoylate PM proteins. One candidate is ACSL1, which appears to directly associate with the FA transporter,

FATP1, at the plasma membrane (75). Clear experimental support for one or the other of these very different hypotheses will have profound implications. In the former case, physical forces within the PM, related to local membrane tension and membrane protein conformation will be the key to regulation of plasma membrane palmitoylation. In the latter case, local turnover and metabolism of FAs will be central to the local control of plasma membrane palmitoylation and the operation of OMDE.

Acknowledgements. STED microscopy was generously supported by the Peter O'Donnell Jr. Brain Institute NeuroMicroscopy Core. We thank Kate Luby-Phelps of the Quantitative Light Microscopy Core for assistance with STED imaging. We thank Fang-Min Lu for expert technical assistance. Supported by NIH HL119843 and Endowed Professors' Collaborative Research Support from the Charles Y.C. Pak Foundation. We thank Marcel Mettlen (UTSouthwestern Quantitative Light Microscopy Core Facility) for imaging advice.

Reference List

1. T. F. Roth, K. R. Porter, YOLK PROTEIN UPTAKE IN THE OOCYTE OF THE MOSQUITO AEDES AEGYPTI. L. *J Cell Biol* **20**, 313-332 (1964).
2. J. L. Goldstein, R. G. Anderson, M. S. Brown, Coated pits, coated vesicles, and receptor-mediated endocytosis. *Nature* **279**, 679-685 (1979).
3. S. A. Doodnauth, S. Grinstein, M. E. Maxson, Constitutive and stimulated macropinocytosis in macrophages: roles in immunity and in the pathogenesis of atherosclerosis. *Philos Trans R Soc Lond B Biol Sci* **374**, 20180147 (2019).
4. Q. Gan, S. Watanabe, Synaptic Vesicle Endocytosis in Different Model Systems. *Front Cell Neurosci* **12**, 171 (2018).
5. G. J. Doherty, H. T. McMahon, Mechanisms of endocytosis. *Annu Rev Biochem* **78**, 857-902 (2009).
6. J. J. Thottacherry, M. Sathe, C. Prabhakara, S. Mayor, Spoiled for Choice: Diverse Endocytic Pathways Function at the Cell Surface. *Annu Rev Cell Dev Biol* **35**, 55-84 (2019).
7. E. Boucrot *et al.*, Endophilin marks and controls a clathrin-independent endocytic pathway. *Nature* **517**, 460-465 (2015).
8. E. Larsson, B. Morén, K. A. McMahon, R. G. Parton, R. Lundmark, Dynamin2 functions as an accessory protein to reduce the rate of caveola internalization. *J Cell Biol* **222** (2023).
9. V. Bitsikas, I. R. Correa, Jr., B. J. Nichols, Clathrin-independent pathways do not contribute significantly to endocytic flux. *Elife* **3**, e03970 (2014).
10. R. J. Park *et al.*, Dynamin triple knockout cells reveal off target effects of commonly used dynamin inhibitors. *J Cell Sci* **126**, 5305-5312 (2013).
11. J. Rappaport, R. L. Manthe, M. Solomon, C. Garnacho, S. Muro, A Comparative Study on the Alterations of Endocytic Pathways in Multiple Lysosomal Storage Disorders. *Mol Pharm* **13**, 357-368 (2016).
12. D. W. Hilgemann, M. J. Lin, M. Fine, C. Deisl, On the existence of endocytosis driven by membrane phase separations. *Biochim Biophys Acta Biomembr* **1862**, 183007 (2020).
13. P. Lajoie, I. R. Nabi, Regulation of raft-dependent endocytosis. *J Cell Mol Med* **11**, 644-653 (2007).
14. M. T. Howes *et al.*, Clathrin-independent carriers form a high capacity endocytic sorting system at the leading edge of migrating cells. *J Cell Biol* **190**, 675-691 (2010).
15. Y. Wu *et al.*, A dynamin 1-, dynamin 3- and clathrin-independent pathway of synaptic vesicle recycling mediated by bulk endocytosis. *Elife* **3**, e01621 (2014).
16. A. G. Tahiliani, Dependence of mitochondrial coenzyme A uptake on the membrane electrical gradient. *J Biol Chem* **264**, 18426-18432 (1989).
17. A. G. Tahiliani, Evidence for net uptake and efflux of mitochondrial coenzyme A. *Biochim Biophys Acta* **1067**, 29-37 (1991).
18. Y. Li, B. R. Martin, B. F. Cravatt, S. L. Hofmann, DHHC5 protein palmitoylates flotillin-2 and is rapidly degraded on induction of neuronal differentiation in cultured cells. *J Biol Chem* **287**, 523-530 (2012).
19. M. J. Lin *et al.*, Massive palmitoylation-dependent endocytosis during reoxygenation of anoxic cardiac muscle. *Elife* **2**, e01295 (2013).
20. B. L. R. Edelman, E.F., " Isolation and Characterization of Mouse Fibroblasts." in Lung Innate Immunity and Inflammation. Methods in Molecular Biology, S. J. Alper, W., Ed. (Humana Press, New York, NY, 2018), vol. 1809.

21. R. Mendoza *et al.*, Mouse Bone Marrow Cell Isolation and Macrophage Differentiation. *Methods Mol Biol* **2455**, 85-91 (2022).
22. A. De Jesus *et al.*, Optimized protocol to isolate primary mouse peritoneal macrophage metabolites. *STAR Protoc* **3**, 101668 (2022).
23. T. M. Wang, D. W. Hilgemann, Ca-dependent nonsecretory vesicle fusion in a secretory cell. *J Gen Physiol* **132**, 51-65 (2008).
24. C. Deisl, M. Fine, O. W. Moe, D. W. Hilgemann, Hypertrophy of human embryonic stem cell-derived cardiomyocytes supported by positive feedback between Ca(2+) and diacylglycerol signals. *Pflugers Arch* **471**, 1143-1157 (2019).
25. J. Noritake *et al.*, Mobile DHHC palmitoylating enzyme mediates activity-sensitive synaptic targeting of PSD-95. *J Cell Biol* **186**, 147-160 (2009).
26. L. Wang *et al.*, Multiphase coalescence mediates Hippo pathway activation. *Cell* **185**, 4376-4393.e4318 (2022).
27. C. Deisl, J. H. Chung, D. W. Hilgemann, Longitudinal diffusion barriers imposed by myofilaments and mitochondria in murine cardiac myocytes. *J Gen Physiol* **155** (2023).
28. L. Reilly *et al.*, Palmitoylation of the Na/Ca exchanger cytoplasmic loop controls its inactivation and internalization during stress signaling. *FASEB J* **29**, 4532-4543 (2015).
29. C. Salaun, J. Greaves, L. H. Chamberlain, The intracellular dynamic of protein palmitoylation. *J Cell Biol* **191**, 1229-1238 (2010).
30. Y. Fukata *et al.*, Local palmitoylation cycles define activity-regulated postsynaptic subdomains. *J Cell Biol* **202**, 145-161 (2013).
31. J. Howie *et al.*, Substrate recognition by the cell surface palmitoyl transferase DHHC5. *Proc Natl Acad Sci U S A* **111**, 17534-17539 (2014).
32. S. Eaton *et al.*, Carnitine palmitoyl transferase I and the control of myocardial beta-oxidation flux. *Biochem Soc Trans* **29**, 245-250 (2001).
33. S. Boulant, C. Kural, J. C. Zeeh, F. Ubelmann, T. Kirchhausen, Actin dynamics counteract membrane tension during clathrin-mediated endocytosis. *Nat Cell Biol* **13**, 1124-1131 (2011).
34. J. Weischenfeldt, B. Porse, Bone Marrow-Derived Macrophages (BMM): Isolation and Applications. *CSH Protoc* **2008**, pdb prot5080 (2008).
35. J. Šileikytė, M. Forte, Shutting down the pore: The search for small molecule inhibitors of the mitochondrial permeability transition. *Biochim Biophys Acta* **1857**, 1197-1202 (2016).
36. C. M. Krishna *et al.*, The catecholic metal sequestering agent 1,2-dihydroxybenzene-3,5-disulfonate confers protection against oxidative cell damage. *Arch Biochem Biophys* **294**, 98-106 (1992).
37. K. Tieu *et al.*, D-beta-hydroxybutyrate rescues mitochondrial respiration and mitigates features of Parkinson disease. *J Clin Invest* **112**, 892-901 (2003).
38. A. C. Caritá, B. Mattei, C. C. Domingues, E. de Paula, K. A. Riske, Effect of Triton X-100 on Raft-Like Lipid Mixtures: Phase Separation and Selective Solubilization. *Langmuir* **33**, 7312-7321 (2017).
39. N. D. Oakes *et al.*, Development and initial evaluation of a novel method for assessing tissue-specific plasma free fatty acid utilization in vivo using (R)-2-bromopalmitate tracer. *J Lipid Res* **40**, 1155-1169 (1999).
40. B. C. Jennings *et al.*, 2-Bromopalmitate and 2-(2-hydroxy-5-nitro-benzylidene)-benzo[b]thiophen-3-one inhibit DHHC-mediated palmitoylation in vitro. *J Lipid Res* **50**, 233-242 (2009).
41. K. M. Broekemeier, M. E. Dempsey, D. R. Pfeiffer, Cyclosporin A is a potent inhibitor of the inner membrane permeability transition in liver mitochondria. *J Biol Chem* **264**, 7826-7830 (1989).

42. D. W. Hilgemann, M. Fine, M. E. Linder, B. C. Jennings, M. J. Lin, Massive endocytosis triggered by surface membrane palmitoylation under mitochondrial control in BHK fibroblasts. *Elife* **2**, e01293 (2013).
43. S.-A. L. Azizi, T; Delalande,C; Kathayat, R; Dickinson, B, Development of an Acrylamide-Based Inhibitor of Protein S-Acylation. *ChemRxiv* https://doi.org/10.26434/chemrxiv.13755763.v1, 66 (2021).
44. A. J. Santiago-Lopez, C. A. Gutekunst, R. E. Gross, C3 Transferase Gene Therapy for Continuous RhoA Inhibition. *Methods Mol Biol* **1821**, 267-281 (2018).
45. P. R. O'Neill *et al.*, Membrane Flow Drives an Adhesion-Independent Amoeboid Cell Migration Mode. *Dev Cell* **46**, 9-22 e24 (2018).
46. P. Rojas-Morales, J. Pedraza-Chaverri, E. Tapia, Ketone bodies, stress response, and redox homeostasis. *Redox Biol* **29**, 101395 (2020).
47. R. Tewari, S. J. West, B. Shayahati, A. M. Akimzhanov, Detection of Protein S-Acylation using Acyl-Resin Assisted Capture. *J Vis Exp* 10.3791/61016 (2020).
48. V. Lariccia *et al.*, Massive calcium-activated endocytosis without involvement of classical endocytic proteins. *J Gen Physiol* **137**, 111-132 (2011).
49. D. J. Chinnapen, H. Chinnapen, D. Saslowsky, W. I. Lencer, Rafting with cholera toxin: endocytosis and trafficking from plasma membrane to ER. *FEMS Microbiol Lett* **266**, 129-137 (2007).
50. M. L. Torgersen, G. Skretting, B. van Deurs, K. Sandvig, Internalization of cholera toxin by different endocytic mechanisms. *J Cell Sci* **114**, 3737-3747 (2001).
51. A. Dautry-Varsat, Receptor-mediated endocytosis: the intracellular journey of transferrin and its receptor. *Biochimie* **68**, 375-381 (1986).
52. S. Q. Jing, I. S. Trowbridge, Nonacylated human transferrin receptors are rapidly internalized and mediate iron uptake. *J Biol Chem* **265**, 11555-11559 (1990).
53. J. Heine *et al.*, Adaptive-illumination STED nanoscopy. *Proc Natl Acad Sci U S A* **114**, 9797-9802 (2017).
54. R. R. Kay, Macropinocytosis: Biology and mechanisms. *Cells Dev* **168**, 203713 (2021).
55. S. Mayor, R. E. Pagano, Pathways of clathrin-independent endocytosis. *Nat Rev Mol Cell Biol* **8**, 603-612 (2007).
56. M. Fine *et al.*, Massive endocytosis driven by lipidic forces originating in the outer plasmalemmal monolayer: a new approach to membrane recycling and lipid domains. *J Gen Physiol* **137**, 137-154 (2011).
57. T. H. Nguyen, X. Qiu, J. Sun, F. A. Meunier, Bulk endocytosis at neuronal synapses. *Sci China Life Sci* **57**, 378-383 (2014).
58. E. Ferro, L. Goitre, S. F. Retta, L. Trabalzini, The Interplay between ROS and Ras GTPases: Physiological and Pathological Implications. *J Signal Transduct* **2012**, 365769 (2012).
59. U. De Marchi, L. Biasutto, S. Garbisa, A. Toninello, M. Zoratti, Quercetin can act either as an inhibitor or an inducer of the mitochondrial permeability transition pore: A demonstration of the ambivalent redox character of polyphenols. *Biochim Biophys Acta* **1787**, 1425-1432 (2009).
60. H. H. Szeto, Cell-permeable, mitochondrial-targeted, peptide antioxidants. *Aaps j* **8**, E277-283 (2006).
61. D. C. Shippy, C. Wilhelm, P. A. Viharkumar, T. J. Raife, T. K. Ulland, β-Hydroxybutyrate inhibits inflammasome activation to attenuate Alzheimer's disease pathology. *J Neuroinflammation* **17**, 280 (2020).
62. X. Wang *et al.*, Pyruvate protects mitochondria from oxidative stress in human neuroblastoma SK-N-SH cells. *Brain Res* **1132**, 1-9 (2007).

63. A. I. Magee, I. Parmryd, Detergent-resistant membranes and the protein composition of lipid rafts. *Genome Biol* **4**, 234 (2003).
64. P. Marchetti *et al.*, Mitochondrial permeability transition is a central coordinating event of apoptosis. *J Exp Med* **184**, 1155-1160 (1996).
65. R. Endlicher, Z. Drahota, K. Štefková, Z. Červinková, O. Kučera, The Mitochondrial Permeability Transition Pore-Current Knowledge of Its Structure, Function, and Regulation, and Optimized Methods for Evaluating Its Functional State. *Cells* **12** (2023).
66. P. Bernardi *et al.*, Identity, structure, and function of the mitochondrial permeability transition pore: controversies, consensus, recent advances, and future directions. *Cell Death Differ* **30**, 1869-1885 (2023).
67. V. Petronilli *et al.*, Transient and long-lasting openings of the mitochondrial permeability transition pore can be monitored directly in intact cells by changes in mitochondrial calcein fluorescence. *Biophys J* **76**, 725-734 (1999).
68. X. Lu, J. Q. Kwong, J. D. Molkentin, D. M. Bers, Individual Cardiac Mitochondria Undergo Rare Transient Permeability Transition Pore Openings. *Circ Res* **118**, 834-841 (2016).
69. Z. Ying *et al.*, Short-Term Mitochondrial Permeability Transition Pore Opening Modulates Histone Lysine Methylation at the Early Phase of Somatic Cell Reprogramming. *Cell Metab* **28**, 935-945.e935 (2018).
70. J. M. Kralj, D. R. Hochbaum, A. D. Douglass, A. E. Cohen, Electrical spiking in Escherichia coli probed with a fluorescent voltage-indicating protein. *Science* **333**, 345-348 (2011).
71. X. Jin *et al.*, Sensitive bacterial V(m) sensors revealed the excitability of bacterial V(m) and its role in antibiotic tolerance. *Proc Natl Acad Sci U S A* **120**, e2208348120 (2023).
72. I. De, S. Sadhukhan, Emerging Roles of DHHC-mediated Protein S-palmitoylation in Physiological and Pathophysiological Context. *Eur J Cell Biol* **97**, 319-338 (2018).
73. R. Lakshminarayan *et al.*, Galectin-3 drives glycosphingolipid-dependent biogenesis of clathrin-independent carriers. *Nat Cell Biol* **16**, 595-606 (2014).
74. T. Meierhofer, J. M. van den Elsen, P. J. Cameron, X. Muñoz-Berbel, A. T. Jenkins, The interaction of serum albumin with cholesterol containing lipid vesicles. *J Fluoresc* **20**, 371-376 (2010).
75. E. Soupene, F. A. Kuypers, Mammalian long-chain acyl-CoA synthetases. *Exp Biol Med (Maywood)* **233**, 507-521 (2008).
76. J. A. Idell-Wenger, L. W. Grotyohann, J. R. Neely, Coenzyme A and carnitine distribution in normal and ischemic hearts. *J Biol Chem* **253**, 4310-4318 (1978).
77. R. Leonardi, Y. M. Zhang, C. O. Rock, S. Jackowski, Coenzyme A: back in action. *Prog Lipid Res* **44**, 125-153 (2005).
78. F. Pietrocola, L. Galluzzi, J. M. Bravo-San Pedro, F. Madeo, G. Kroemer, Acetyl coenzyme A: a central metabolite and second messenger. *Cell Metab* **21**, 805-821 (2015).
79. D. Hausenloy, A. Wynne, M. Duchen, D. Yellon, Transient mitochondrial permeability transition pore opening mediates preconditioning-induced protection. *Circulation* **109**, 1714-1717 (2004).
80. J. W. Hao *et al.*, CD36 facilitates fatty acid uptake by dynamic palmitoylation-regulated endocytosis. *Nat Commun* **11**, 4765 (2020).
81. I. Levental, D. Lingwood, M. Grzybek, U. Coskun, K. Simons, Palmitoylation regulates raft affinity for the majority of integral raft proteins. *Proc Natl Acad Sci U S A* **107**, 22050-22054 (2010).
82. S. P. Thankamony, W. Knudson, Acylation of CD44 and its association with lipid rafts are required for receptor and hyaluronan endocytosis. *J Biol Chem* **281**, 34601-34609 (2006).
83. Y. Zeng, N. Tao, K. N. Chung, J. E. Heuser, D. M. Lublin, Endocytosis of oxidized low density lipoprotein through scavenger receptor CD36 utilizes a lipid raft pathway that does not require caveolin-1. *J Biol Chem* **278**, 45931-45936 (2003).

84. R. Knorr, C. Karacsonyi, R. Lindner, Endocytosis of MHC molecules by distinct membrane rafts. *J Cell Sci* **122**, 1584-1594 (2009).
85. A. Wittrup *et al.*, Magnetic nanoparticle-based isolation of endocytic vesicles reveals a role of the heat shock protein GRP75 in macromolecular delivery. *Proc Natl Acad Sci U S A* **107**, 13342-13347 (2010).
86. I. Ripa, S. Andreu, J. A. López-Guerrero, R. Bello-Morales, Membrane Rafts: Portals for Viral Entry. *Front Microbiol* **12**, 631274 (2021).
87. T. Sorkina, S. Ma, M. B. Larsen, S. C. Watkins, A. Sorkin, Small molecule induced oligomerization, clustering and clathrin-independent endocytosis of the dopamine transporter. *Elife* **7** (2018).
88. C. Deisl, D. W. Hilgemann, R. Syeda, M. Fine, TMEM16F and dynamins control expansive plasma membrane reservoirs. *Nat Commun* **12**, 4990 (2021).
89. H. H. Kerschbaum, B. A. Tasa, M. Schürz, K. Oberascher, N. Bresgen, Trypan Blue - Adapting a Dye Used for Labelling Dead Cells to Visualize Pinocytosis in Viable Cells. *Cell Physiol Biochem* **55**, 171-184 (2021).

Figure Legends.

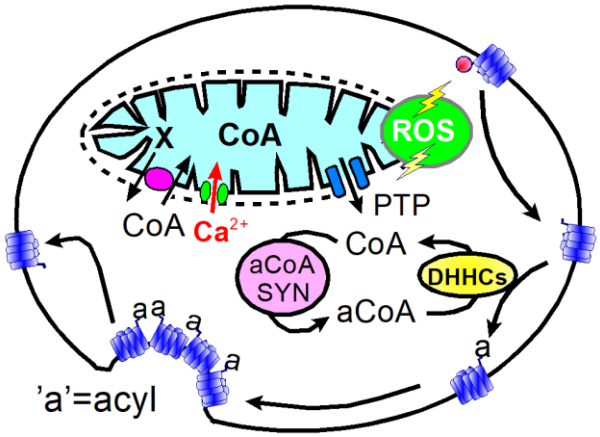

Figure 1. Working hypotheses. Mitochondria accumulate coenzyme A to a high concentration with respect to cytoplasm and release it during metabolic stress, for example during post-ischemic stress (19, 76). Cytoplasmic coenzyme A (77) and acetyl-coenzyme A (78) concentrations fluctuate enough to influence enzymes that use them as cofactors and substrates. Thus, both molecules have second messenger functions. Coenzyme A is released from mitochondria via transient openings of permeability transition pores (PTPs) that occur physiologically as mitochondria accumulate Ca and oxidize critical cysteines (e.g. (79)). Elevations of cytoplasmic coenzyme A promote acyl-CoA synthesis and subsequently DHHC acyltransferase activity. DHHC-mediated palmitoylations are regulated by small G-proteins that modify membrane cytoskeleton function, ROS signaling, phosphorylations (80), and conformational changes of the PM and PM proteins. Reversible palmitoylations of membrane proteins can promote their coalescence into ordered membrane domains, commonly called 'rafts', thereby supporting the budding of ordered domains inwardly to ultimately form endocytic vesicles (81). Palmitoylation-dependent ordered membrane domain endocytosis (OMDE) is long known to mediate uptake of proteins and particles by cells. Examples include the uptake of hyaluronic acid by CD44 (82), uptake of oxidized LDL and fatty acids by CD36 (83), uptake of nanoparticles and proteins by heparan sulfate proteoglycan receptors (84, 85), and uptake of multiple viruses (86). Additionally, the clustering of some membrane transporters, independent of ligands, promotes their endocytosis in a cargo-dependent manner without involvement of classical endocytic proteins (28, 87).

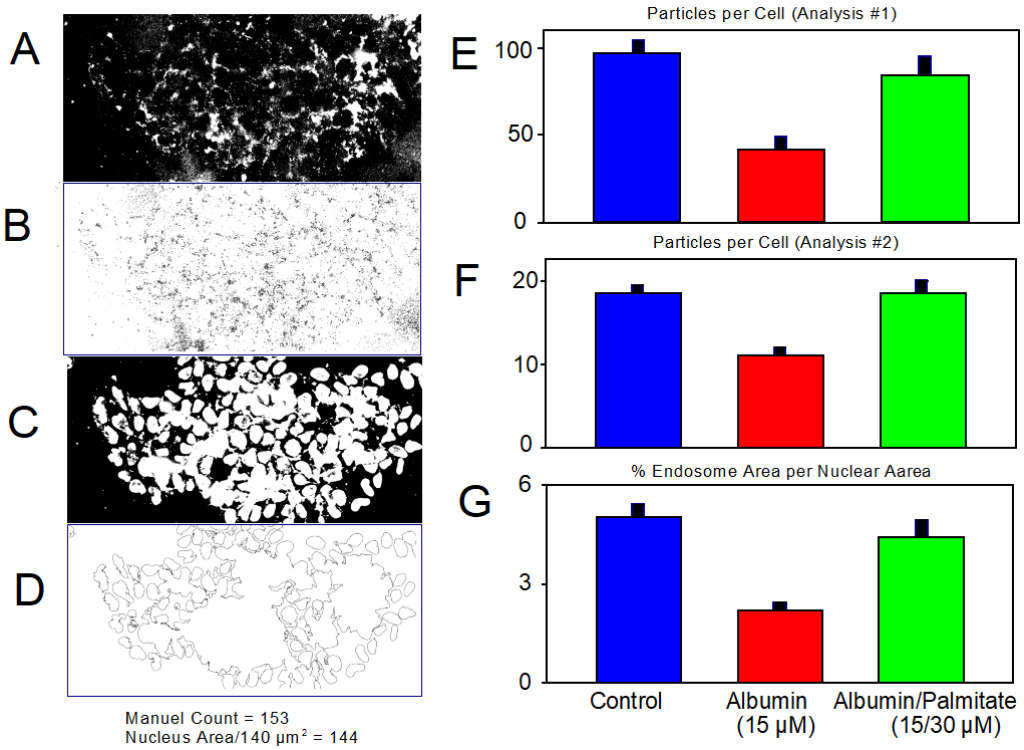

Figure 2. Analysis of 3kD TexasRed™-dextran uptake into T-REx293 cells for 4 min. To determine cell numbers, cells were labelled with Hoechst 33343 dye after terminating uptake with cold solution. We illustrate our analysis via ImageJ software using an example in which cells are distributed unevenly and partially very densely. **A.** Fluroescence image of the dextran taken up with a threshold set to exclude autofluorescence. **B.** Outlines of all punctae rendered by ImageJ up to a maximal particle size of 2 square microns. We note that the lower threshold limit excludes light from the edges of puncta, resulting in a compression of puncta dimensions. Therefore, we do not enforce a lower limit on puncta dimensions. **C.** Image of Hoechst-stained nuclei for the same field of view. A manual count of nuclei yielded a value of 153. **D.** Image of nuclei borders determined by ImageJ. Typical for fields with a high cell density, the outlined of neighboring nuclei merge so that automated nuclei counting is inaccurate. Therefore, we determined the total nuclear area from these outlines and divided by an average nucleus area, determined from >50 measurements, to estimate the total number of cells in the image. The estimate was

144. Similar to 5 other test cases, the differences between this automated cell count and manual counts was less than 10% . **E-G.** Representative analysis of dextran uptake, namely the effect of albumin (15 µM) and albumin/palmitate (15/30 µM) on dextran uptake described in Fig. 7. **E**. Particle counts per cell, determined as in in panels A-D. Average particle counts for 4 min dextran uptake were ~100 particles per cell. Counts were 63% after albumin exposure, while they are only marginally decreased after albumin/palmitate complex exposure. **F.** Particle counts with minimum particle diameter set to 0.2 microns. Control particle counts are reduced to about 20 per cell when the size limit is set to the wavelength of light. As described in Fig. 9, analysis with STED microscopy verifies that particle counts without a lower dimension limit are likely more accurate. We note additionally that the imposition of a lower particle size limit may artificially distort the magnitude of the inhibitory effect of albumin (see Panel F versus Panel E). **G.** Representative of more than 20 observations, changes of dye uptake, as accessed by particle counts, are essentially the same when dye uptake is quantified as endosome (particle) area per total nuclear area.

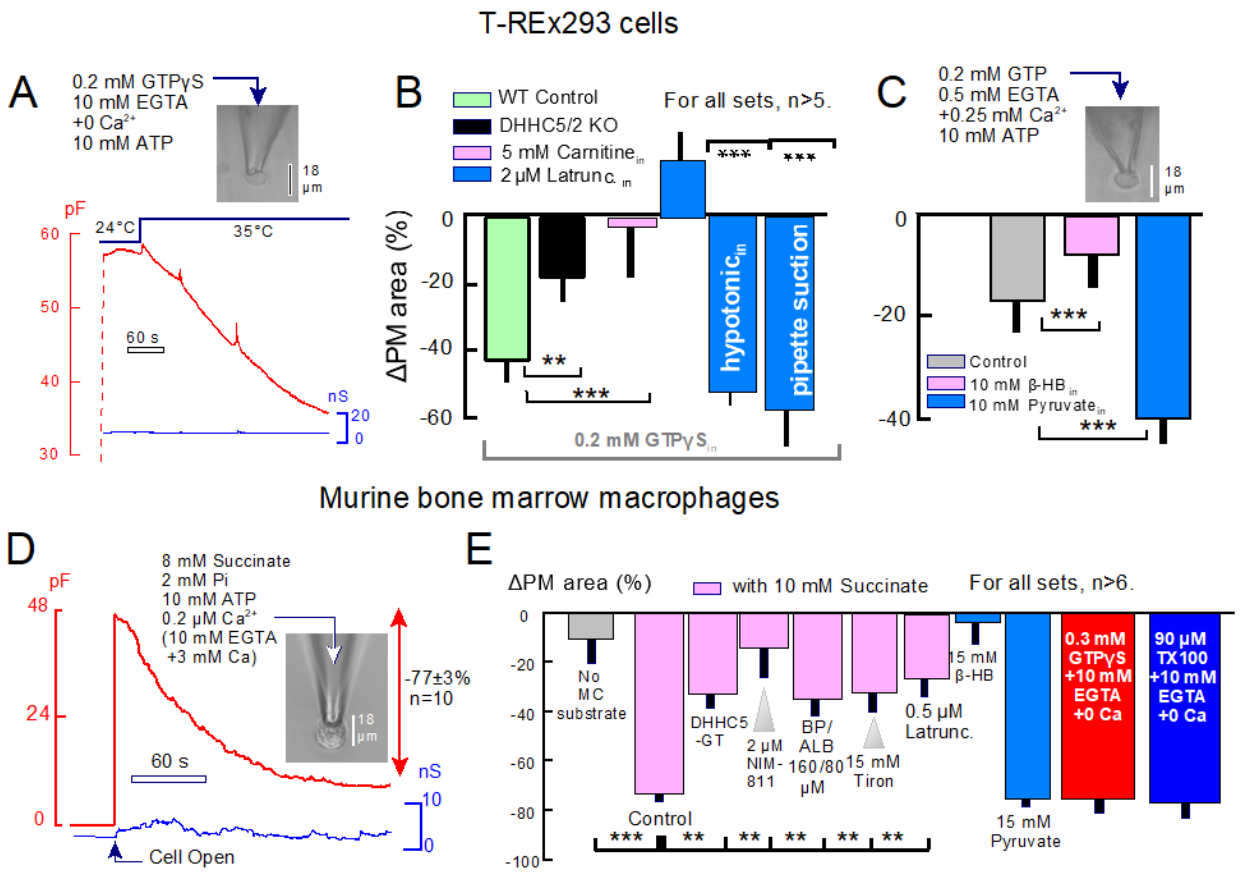

Figure 3. Patch clamp analysis of OMDE activated by cytoplasmic GTPγS and by mitochondrial substrates (succinate or pyruvate) in T-REx293 cells (A-C) and in cultured murine bone marrow macrophages (BMMs, D-E). **A.** Typical recording of T-REx293 cell capacitance (red) and conductance (blue) after cell rupture in the presence of GTPγS (2 mM) in the pipette solution with 10 mM EGTA, no added Ca, and 10 mM Mg ATP. Upon moving the cell into a warm solution stream (35°C), cell capacitance (i.e. PM area) begins to fall within seconds and decreases by 40% over 8 min. Cell conductance remains unchanged. **B.** Composite results for experiments employing the protocol of Panel A. From left to right, average PM loss amounts to 42 % (green), PM loss is decreased from 40% to 18% in a cell line in which the acyltransferases DHHC5 and DHHC2 were deleted by CRSPR (black), PM loss is decreased by 90% when 5 mM carnitine (5 mM) is included in the pipette (pink), and PM loss is not only blocked, but replaced by a small PM expansion response, when latrunculin (2 µM) is included in the pipette (blue). The effect of latrunculin is entirely reversed by promoting cell shrinkage with a 30% hypotonic cytoplasmic solution or by applying enough negative pressure to the pipette to induce just-visible cell

shrinkage (blue). **C.** PM loss after T-REx293 cell opening with a pipette solution containing GTP (0.2 mM), EGTA (0.5 mM) with Ca (0.25 mM, free Ca ≈ 0.3 µM), and MgATP (10 mM). PM loss over 5 min amounts to 18% in control cells. Loss is reduced to 8 % in cells perfused with Na-β-hydroxybutyrate (10 mM), and loss is increased to 40% in cells perfused with 10 mM Na-pyruvate. **D.** Representative record of BMM cell capacitance (red) and conductance (blue) changes upon cell rupture just after the cell was warmed to 35°C. With a pipette solution containing succinate (8 mM), Pi (2 mM), Mg ATP (10 mM) and free Ca clamped to ~0.2 µM (10 mM EGTA with 3 mM Ca), BMM capacitance amounts initially to 48 pF. Capacitance declines over 4 min to ~10 pF with essentially no change of BMM conductance. **E.** From left to right, loss of PM area amounts to only 10% when succinate is not included in the pipette (gray) versus 77% with succinate (pink). PM loss is decreased by 65% in BMMs from animals with gene-trapped DHHC5 acyltransferase (pink), PM loss is decreased 77% when the mitochondria-specific cyclosporin, NIM-811 (2 µM) is included in solutions on both membrane sides (pink). PM loss is decreased by 60% when cells are incubated with brompalmitate/ albumin complexes for 10 min (160/80 µM, pink), decreased by 63% when the antioxidant, tiron (15 mM) was included in the pipette (pink), and decreased 70% when cells were pretreated with latrunculin (0.5 µM) for 10 min (pink). PM loss was less than 10% when the pipette solution contained β-hydroxybutyrate (15 mM), instead of succinate (blue), while pyruvate (15 mM) promoted an equal PM loss to that occurring with succinate. PM loss was similarly large when GTPγS was used to induce OMDE in the absence of mitochondrial substrates. Finally, PM loss was similarly large when rapid application of tritonX-100 (90 µM) was used to induce massive endocytosis by promoting PM phase separations (12).

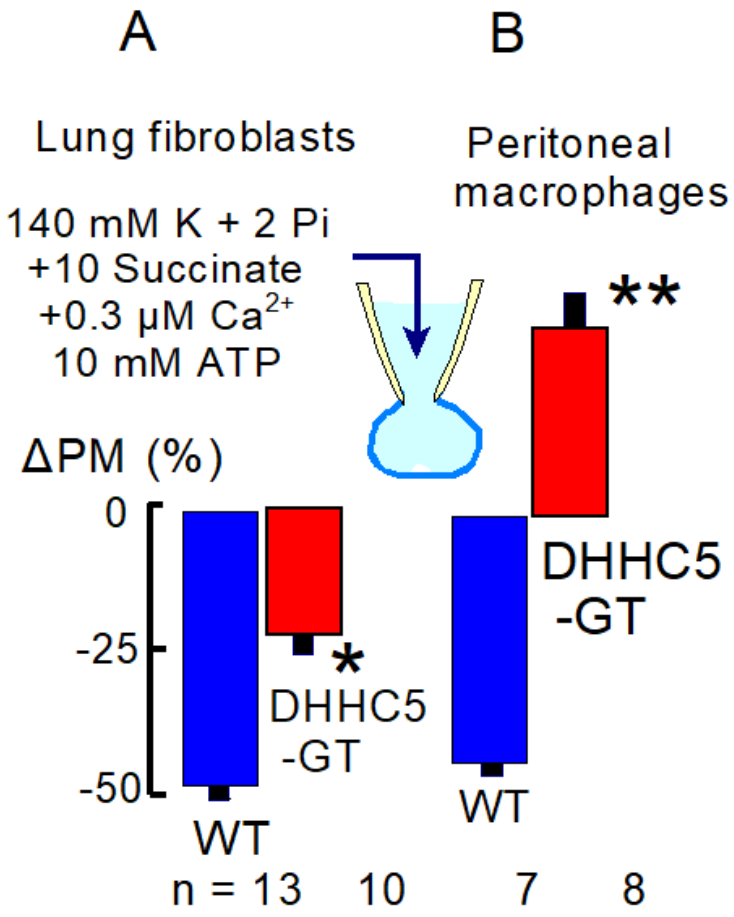

Figure 4. OMDE induced by cytoplasmic succinate in patch-clamped murine lung fibroblasts and acutely isolated peritoneal macrophages under the conditions of Fig. 3E. **Left panel.** OMDE induced by succinate perfusion into lung fibroblasts is reduced by 60% in fibroblasts from animals with gene-trapped DHHC5 (DHHC5-GT). **Right panel.** OMDE induced by succinate perfusion into peritoneal macrophages is blocked and replaced by PM expansion in cells from DHHC5-GT animals.

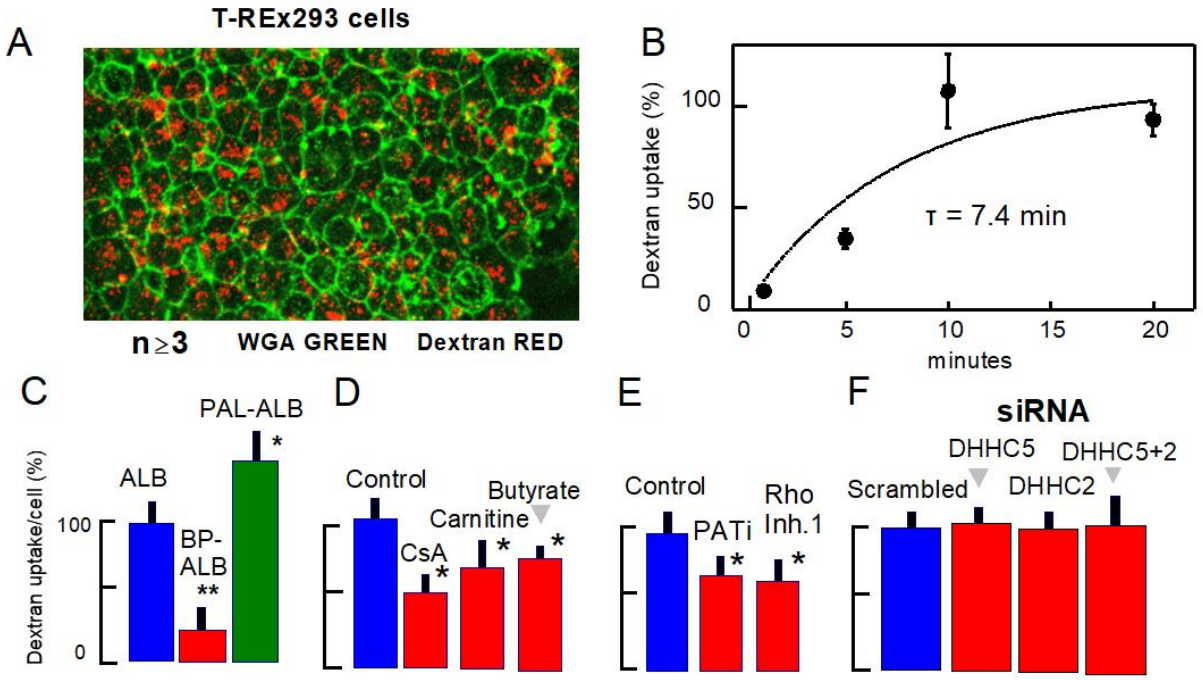

Figure 5. Standard 3kD TexasRed™-dextran uptake assay in a confluent T-REx293 cell culture. **A.** Combined WGA green fluorescence and dextran fluorescence in a culture fixed after 20 min of uptake. Nucleus stain to determine cell numbers is not shown. **B.** The constitutive uptake of dextran saturates over ~20 min, and the apparent time constant is 7.4 min. Therefore, our standard uptake time in subsequent experiments presented was limited to 4 min. **C-F.** Experimental results consistent with a contribution of OMDE under mitochondrial control to constitutive dextran uptake. **C.** Strong inhibition of dextran uptake by bromopalmitate/albumin complexes (0.3/0.1mM, red) versus albumin alone (0.1 mM, blue) and versus uptake stimulation by albumin/palmitate complexes (0.1/0.3 mM, green). **D.** Inhibition of dextran uptake by >50% with cyclosporin A (2 µM), significant inhibition by carnitine (10 mM) and butyrate (10 mM). **E.** Significant inhibition of uptake by a recently developed DHHC inhibitor (PATi) and by Rho-Inhibitor1. **F.** Failure to inhibit dextran uptake by siRNA knockdown of DHHC5, DHHC2 or combined DHHC5/DHHC2 knockdown.

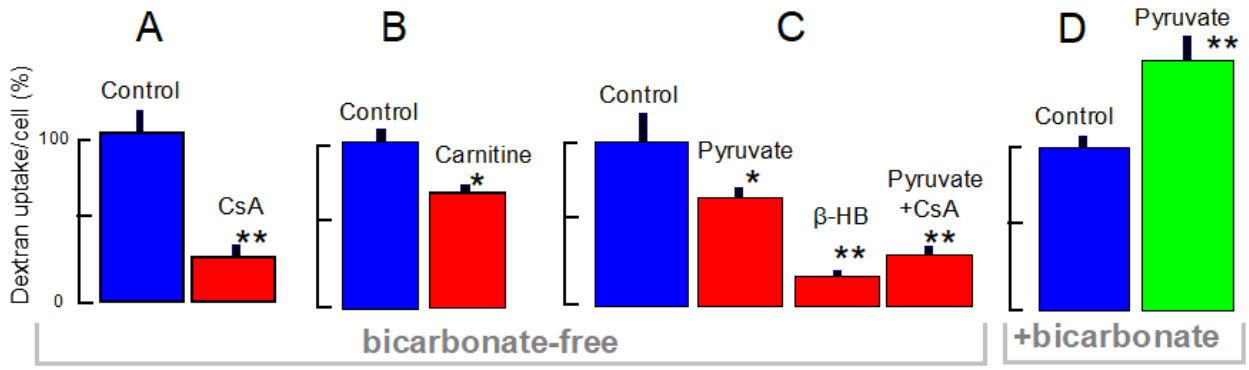

Figure 6. Endocytosis of 3kD TexasRed™-dextran under conditions that progressively support OMDE, namely addition of a mitochondrial substrate (10 mM Na-acetate, A-C) and addition of Na-bicarbonate (25 mM at pH 7.2, D). **A**. Strong inhibition of dextran endocytosis by cyclosporin A (CsA, 1 µM) in the presence of acetate. **B.** Significant inhibition of dextran endocytosis by carnitine (10 mM). **C.** In the presence of acetate without bicarbonate, dextran endocytosis is markedly inhibited by pyruvate (12 mM), strongly inhibited by β-hydroxybutyrate, and markedly inhibited by cyclosporin A (1 µM) in the presence of pyruvate (12 mM). **D.** In the presence of acetate and bicarbonate, dextran endocytosis is strongly stimulated by pyruvate (12 mM).

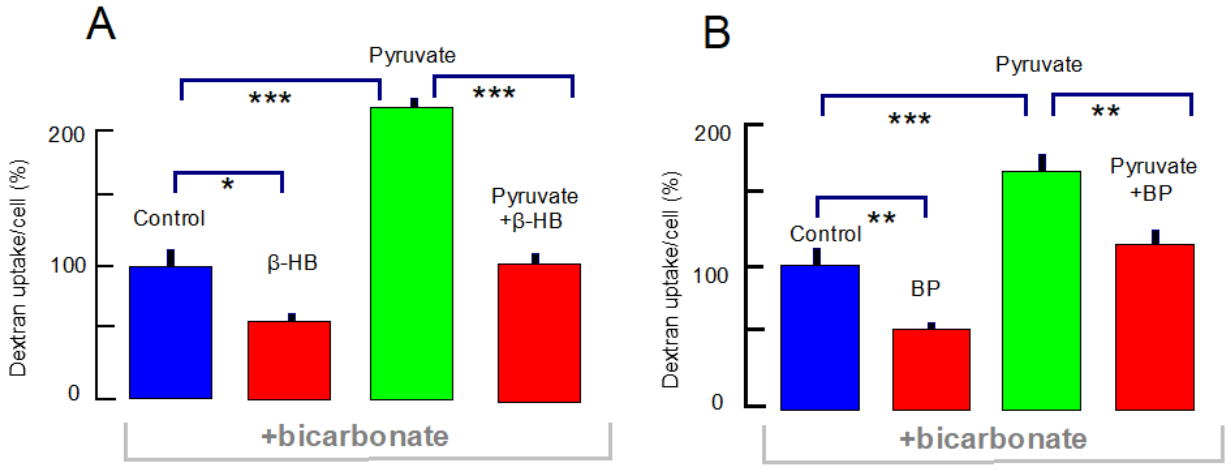

Figure 7. Pyruvate activation of dextran uptake (4 min) is blocked by β-HB and decreased by albumin/bromopalmitate complexes. **A.** β-HB (12 mM), applied for 30 min prior to the uptake assay, inhibit dextran uptake by 50%, while pyruvate (12 mM) enhances dextran uptake by 2.5-fold. The enhancement by pyruvate is effectively blocked by β-HB (12 mM). **B.** Bromopalmitate/albumin complexes (0.2/0.1 mM), applied for 30 min prior to uptake, decrease constitutive endocytosis by ~50% and decrease uptake in the presence of pyruvate by 30%. Note that the inhibition by β-HB is stronger than the inhibition by bromopalmitate/albumin complexes.

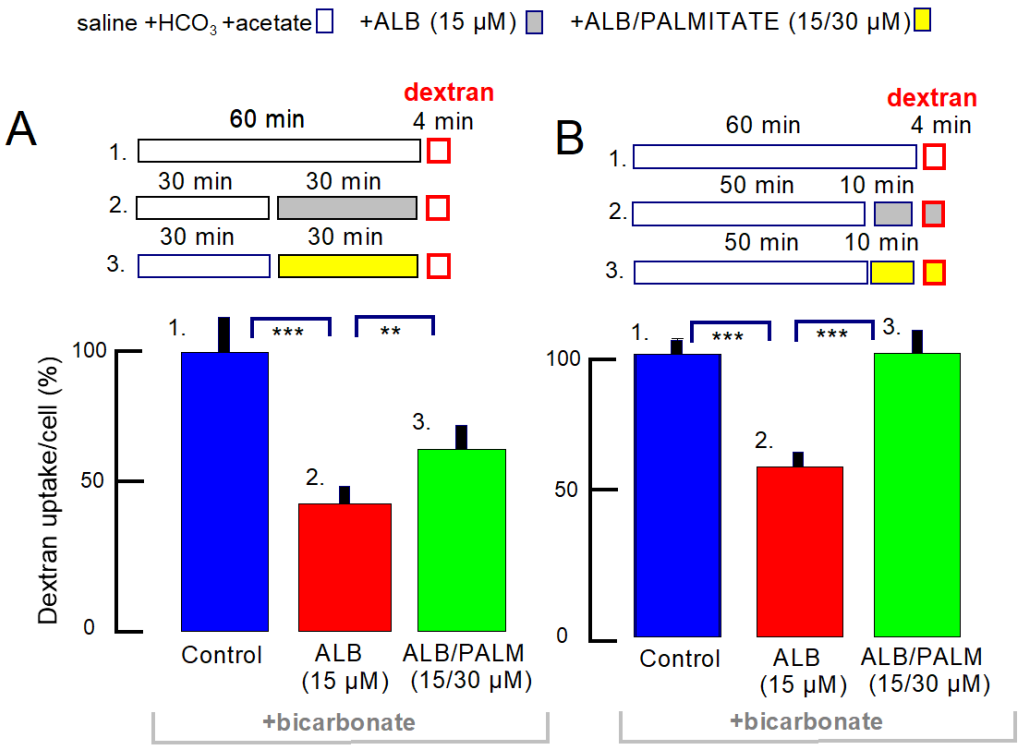

Figure 8. Dextran uptake (4 min with acetate and bicarbonate) is differentially inhibited by low (15 µM) albumin concentrations versus albumin/palmitate complexes (15/30 µM). **A.** As indicated above Panel A, control cells were incubated for 60 min with acetate/bicarbonate-containing saline followed by 4 min dextran uptake ("1"). Second ("2") and third ("3") sets of cells were incubated with saline for 30 min followed by 30 min with 15 µM albumin or 15 µM albumin with 30 µM palmitate. Dextran uptake was then initiated for 4 min in the absence of albumin and palmitate. Albumin exposure inhibited subsequent dextran uptake by >50%. **B.** As indicated above Panel B, control cells were incubated in bicarbonate/acetate-containing saline for 60 min, followed by dextran uptake for 4 min ("1"). Additional sets of cells were incubated for 50 min with saline followed by 10 min with albumin (15 µM) or albumin with palmitate (15 µM/30 µM). Dextran uptake was then initiated for 4 min with albumin or albumin with palmitate, as indicated. The inhibitory effect of albumin alone amounted to 40%, and the presence of palmitate with albumin completely overcame the inhibitory effect of albumin.

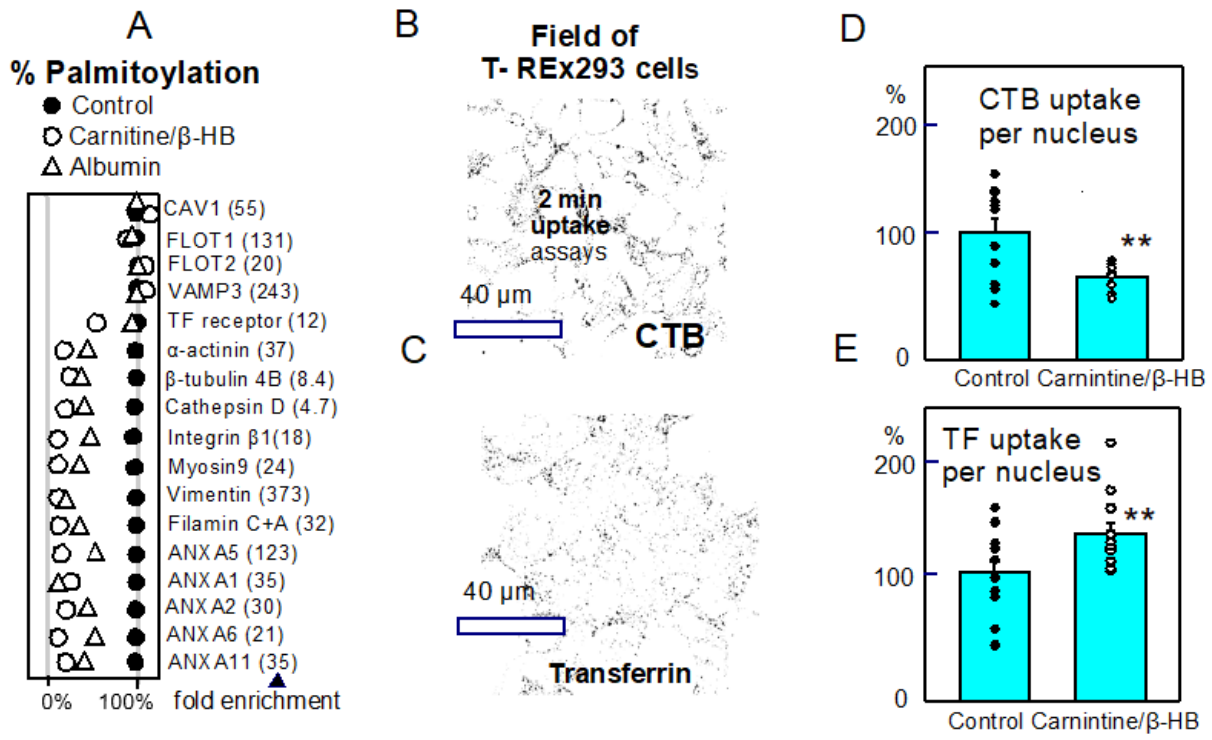

Figure 9. Biochemical and cell biological evidence for selective role of palmitoylation in OMDE. **A.** Carnitine/β-HB and FA-free albumin treatments cause depalmitoylation of numerous membrane proteins. Crude membrane fractions were isolated from control T-REx293 cells and cells treated with carnitine/β-HB (10 mM/10 mM) or FA-free albumin (15 µM). Acyl-RAC protein pull-downs were then analyzed by mass spectometry. As indicated, the palmitoylation of many membrane proteins that are enriched in the depalmitoylated (hydroxylamine-treated) samples is strongly decreased. All of the examples given are represented in the SwissPalm data base multiple times and verified by multiple methods. We note that the palmitoylated proteins that do not change are palmitoylated at multiple sites. **B,C.** **C**holera toxin B (CTB) and transferin (TF) uptake for 2 min in fields of T-REx293 cells, analyzed with Aurox imaging. The micrographs are negative images. **D,E.** Effects of treating cells with carnitine/β-HB (10mM/10mM) for 10 min. TB uptake is decreased s by 37% ($p<0.02$) while TF uptake was increased by 22% ($p<0.01$).

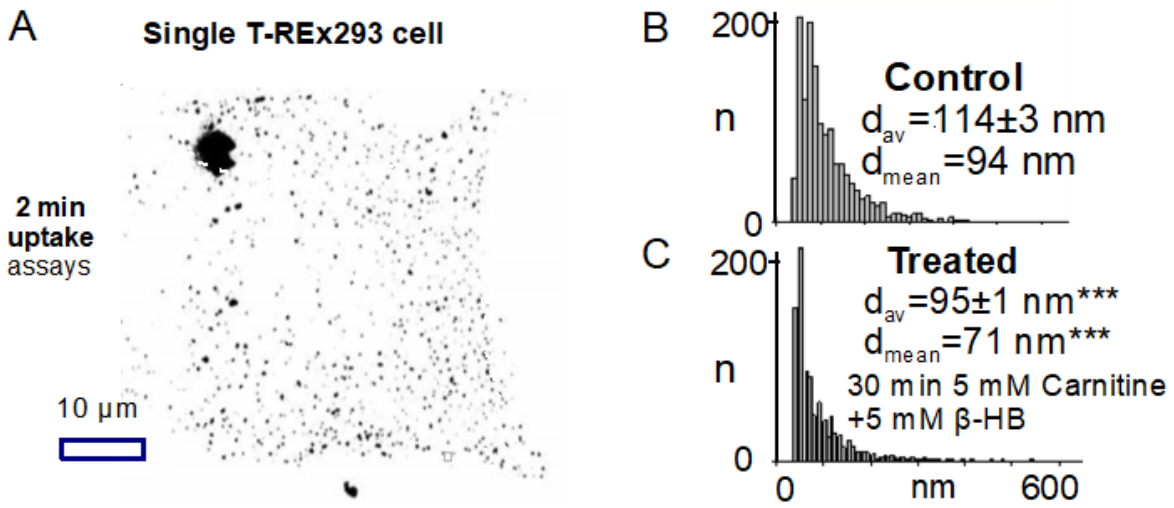

Figure 10. OMDE vesicle dimensions and correlation with palmiatoylation state of membrane proteins in T-REx293 cells. **A.** Negative fluorescence image of a Single T-REx293 cell, visualized with STED microscopy after CF640R dextran uptake for 2 min. Cells were serum/substrate-free for 20 min and fixed after incubation with CF640R dextran for 2 min. STED resolution was determined to be ~30 nm, thereby allowing **a**ccurate quantification of endocytic vesicle dimeters. **B,C.** Histograms of puncta diameters under control conditions and after treatment for 30 min with carnitine/β-HB (5 mM/5 mM) reveal a highly significant decrease of average and mean vesicle sizes. Particle counts within the diameter range of 80 to 140 nm are significantly decreased ($p<0.01$).

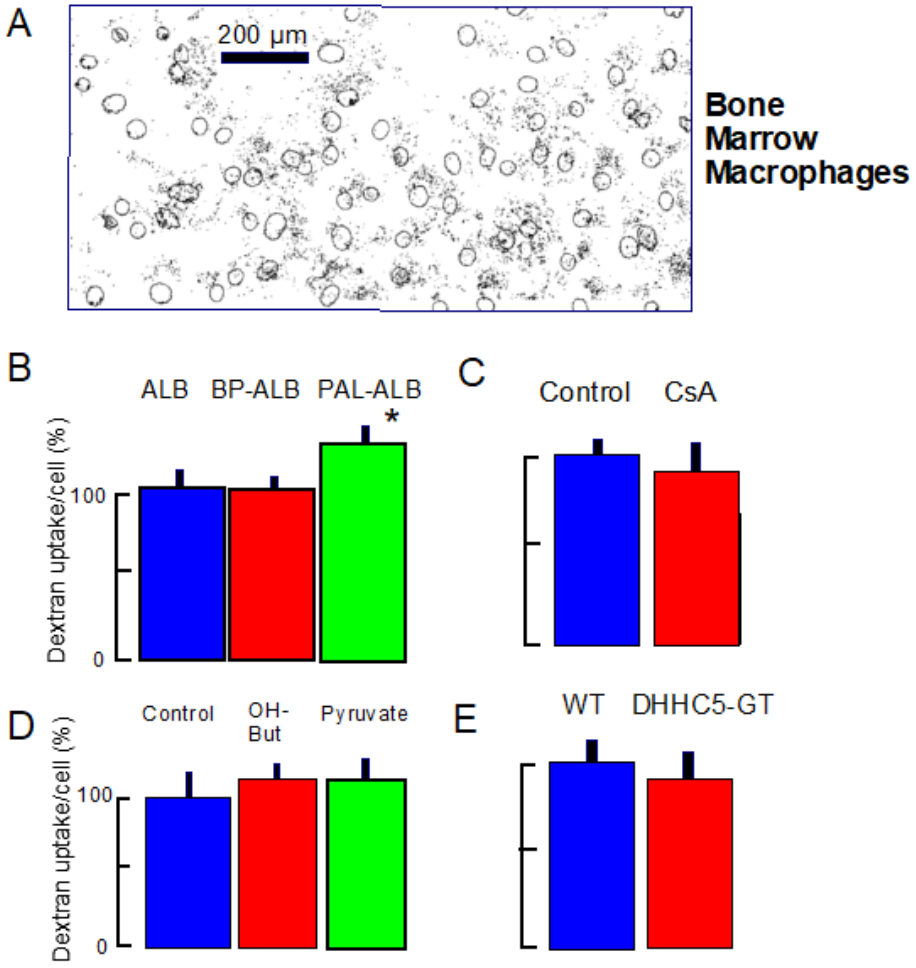

Figure 11. Uptake of TexasRed™-dextran in BMMs, differentiated in cell culture for 7 days, in the absence of serum and metabolic substrates. Particle counts per cell ranged from 30 to 50% of those obtained in T-REx293 cells. **A.** Typical outlines of nuclei (Hoechst dye) and endocytic particles (puncta) determined with Aurox near-confocal imaging after 20 min of TexasRed™-dextran uptake. **B.** In strong contrast to T-REx293 cells under the same condition, bromopalmitate/albumin complexes are not inhibitory, and the stimulatory effect of equivalent palmitate/ albumin complexes is very small. **C.** In stronr contrast to T-REx293 cells under the same condition, cyclosporin A (CsA) is without effect on dextran uptake. **D.** Both β-HB (10 mM) and pyruvate (10 mM) are without effect in BMMs under the conditions of these experiments. **E.** Dextran uptake in BMMs from WT and DHHC5 gene-trapped BMMs is not significantly different.

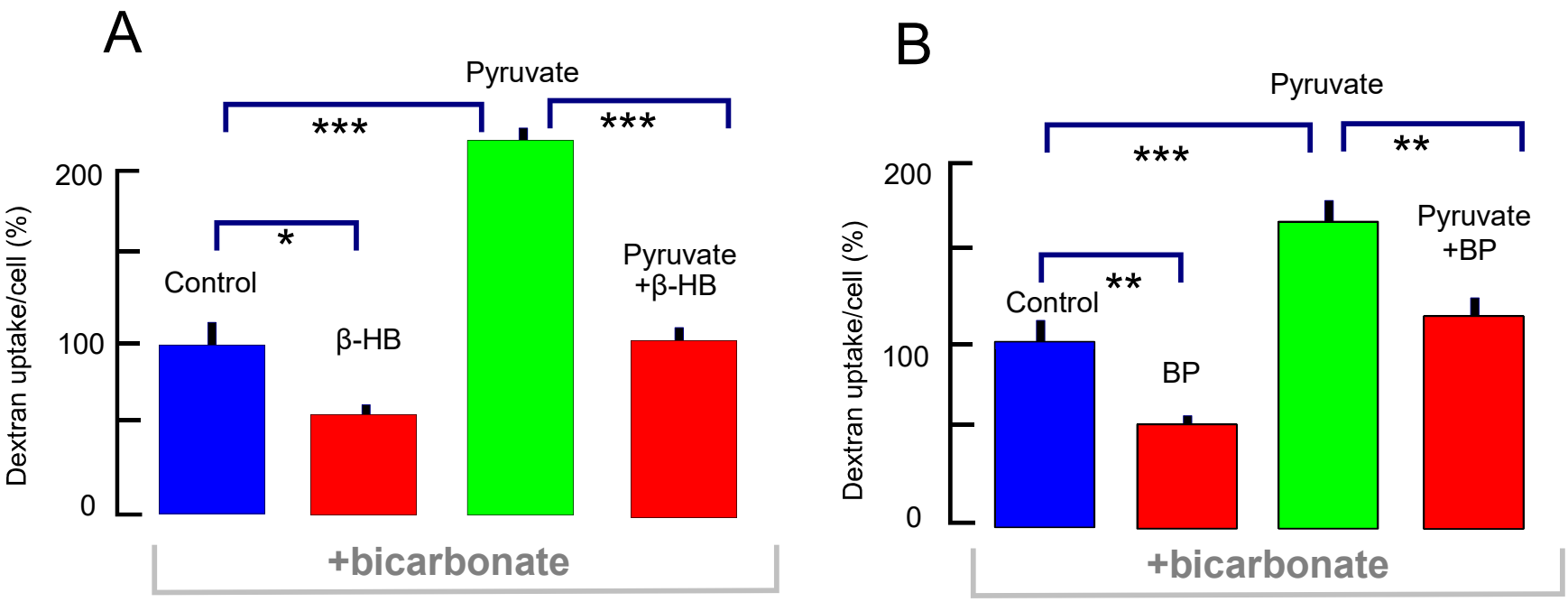
A
Pyruvate
***
***
*
200
100
0
Dextran uptake/cell (%)
Control
β-HB
Pyruvate
+β-HB
+bicarbonate
B
Pyruvate
***
**
**
200
100
0
Dextran uptake/cell (%)
Control
BP
Pyruvate
+BP
+bicarbonate

Figure 7

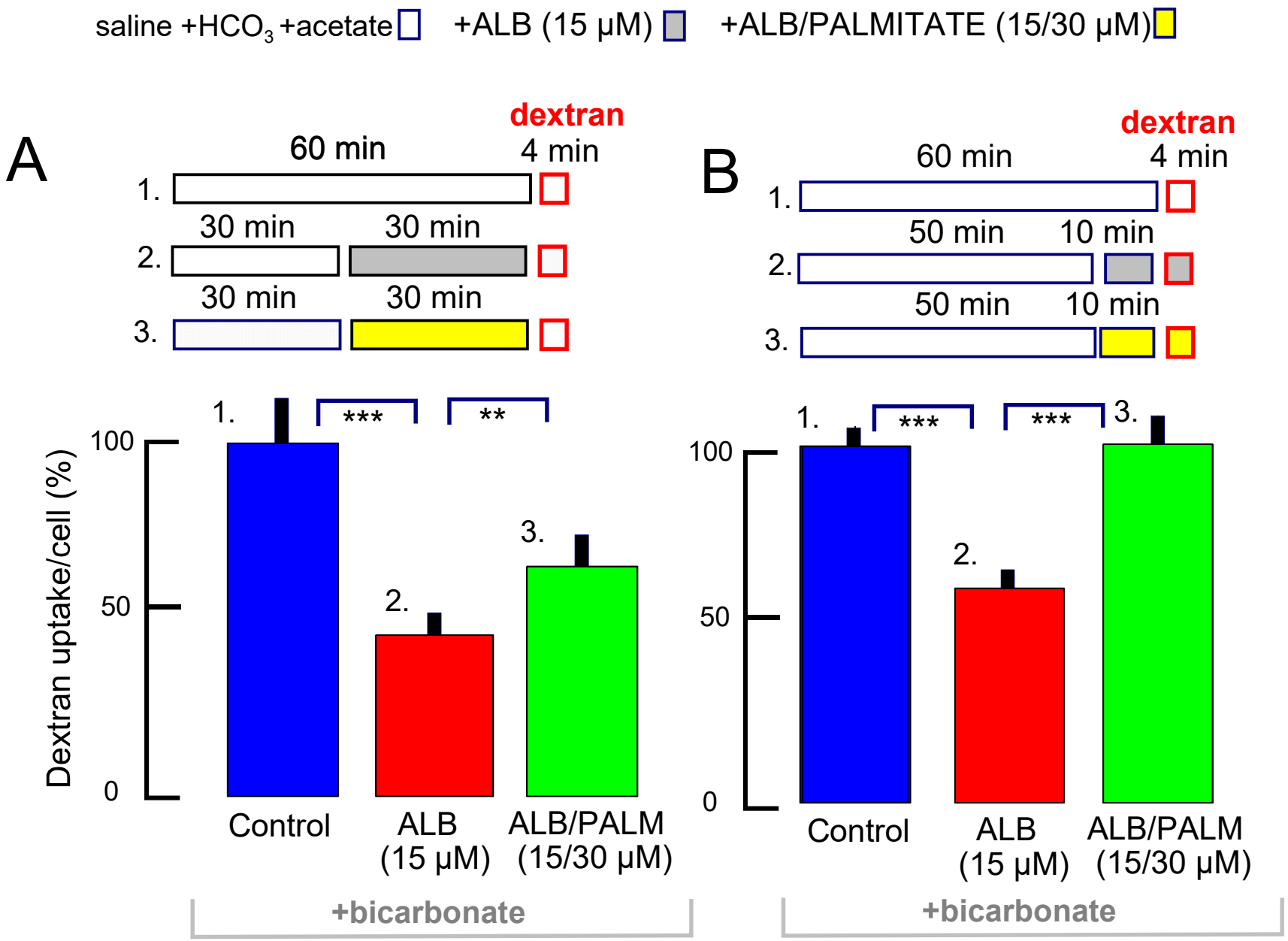
saline +HCO3 +acetate
+ALB (15 μM)
+ALB/PALMITATE (15/30 μM)
A
dextran
60 min
4 min
1.
30 min
30 min
2.
30 min
30 min
3.
Dextran uptake/cell (%)
100
50
0
1.
***
**
2.
3.
Control
ALB
(15 μM)
ALB/PALM
(15/30 μM)
+bicarbonate
B
dextran
60 min
4 min
1.
50 min
10 min
2.
50 min
10 min
3.
100
50
0
1.
***
***
3.
2.
Control
ALB
(15 μM)
ALB/PALM
(15/30 μM)
+bicarbonate

Figure 8

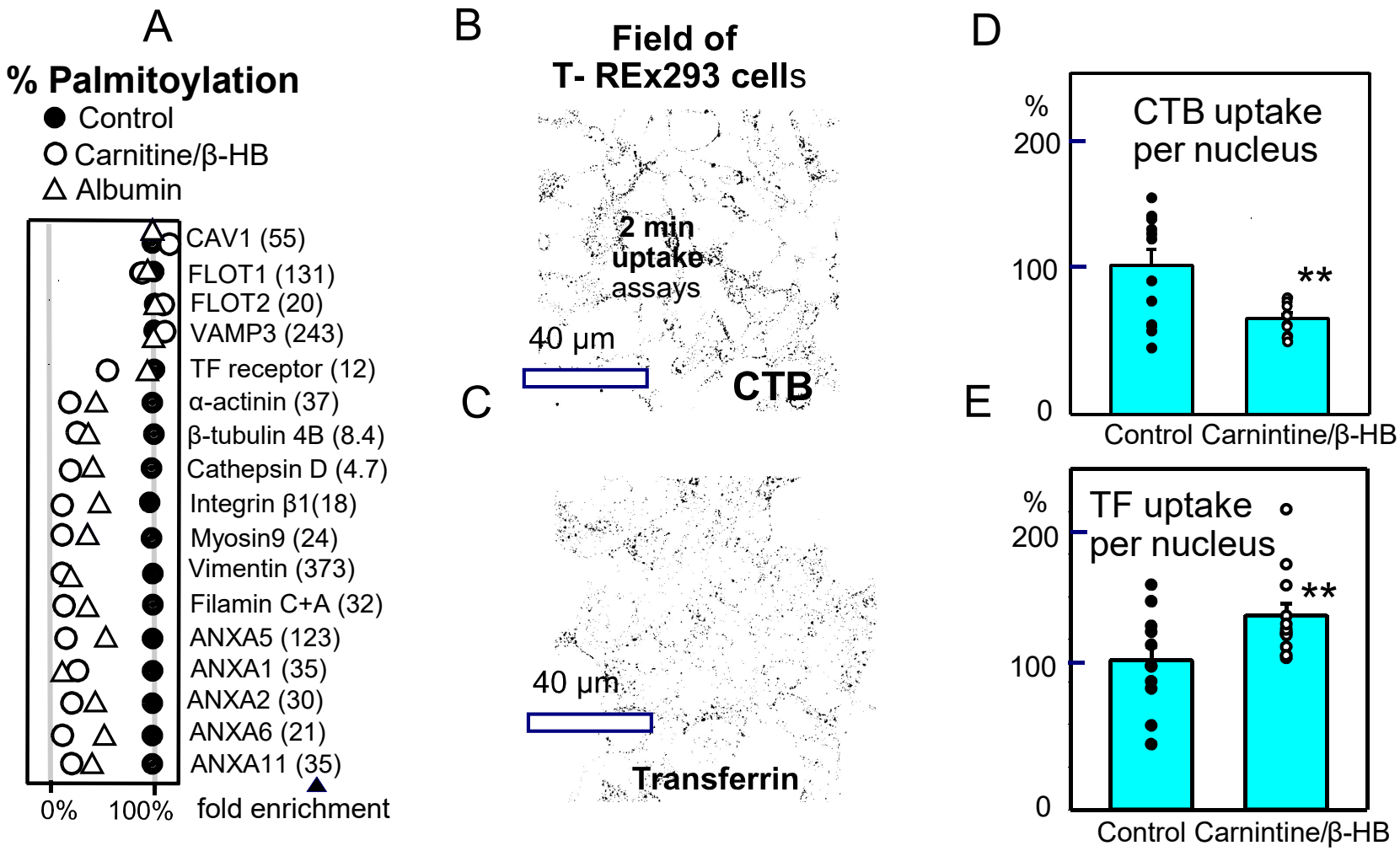
A
% Palmitoylation
Control
Carnitine/β-HB
Albumin
CAV1 (55)
FLOT1 (131)
FLOT2 (20)
VAMP3 (243)
TF receptor (12)
α-actinin (37)
β-tubulin 4B (8.4)
Cathepsin D (4.7)
Integrin β1(18)
Myosin9 (24)
Vimentin (373)
Filamin C+A (32)
ANXA5 (123)
ANXA1 (35)
ANXA2 (30)
ANXA6 (21)
ANXA11 (35)
0%
100%
fold enrichment
B
Field of
T- REx293 cells
2 min
uptake
assays
40 µm
CTB
C
40 µm
Transferrin
D
CTB uptake
per nucleus
%
200
100
0
**
Control
Carnintine/β-HB
E
TF uptake
per nucleus
%
200
100
0
**
Control
Carnintine/β-HB

Figure 9

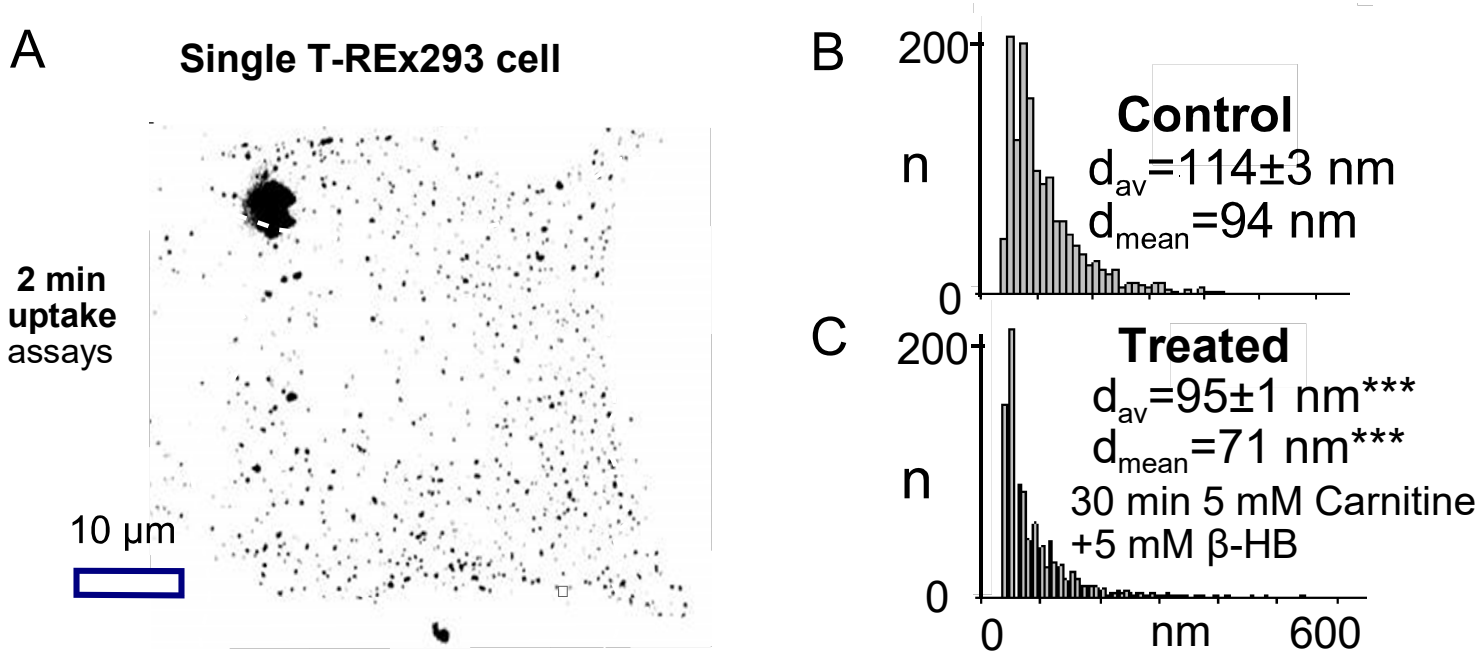
A
Single T-REx293 cell
2 min
uptake
assays
10 µm
B
200
n
0
Control
d_{av}=114±3 nm
d_{mean}=94 nm
C
200
n
0
Treated
d_{av}=95±1 nm***
d_{mean}=71 nm***
30 min 5 mM Carnitine
+5 mM β-HB
0
nm
600

Figure 10

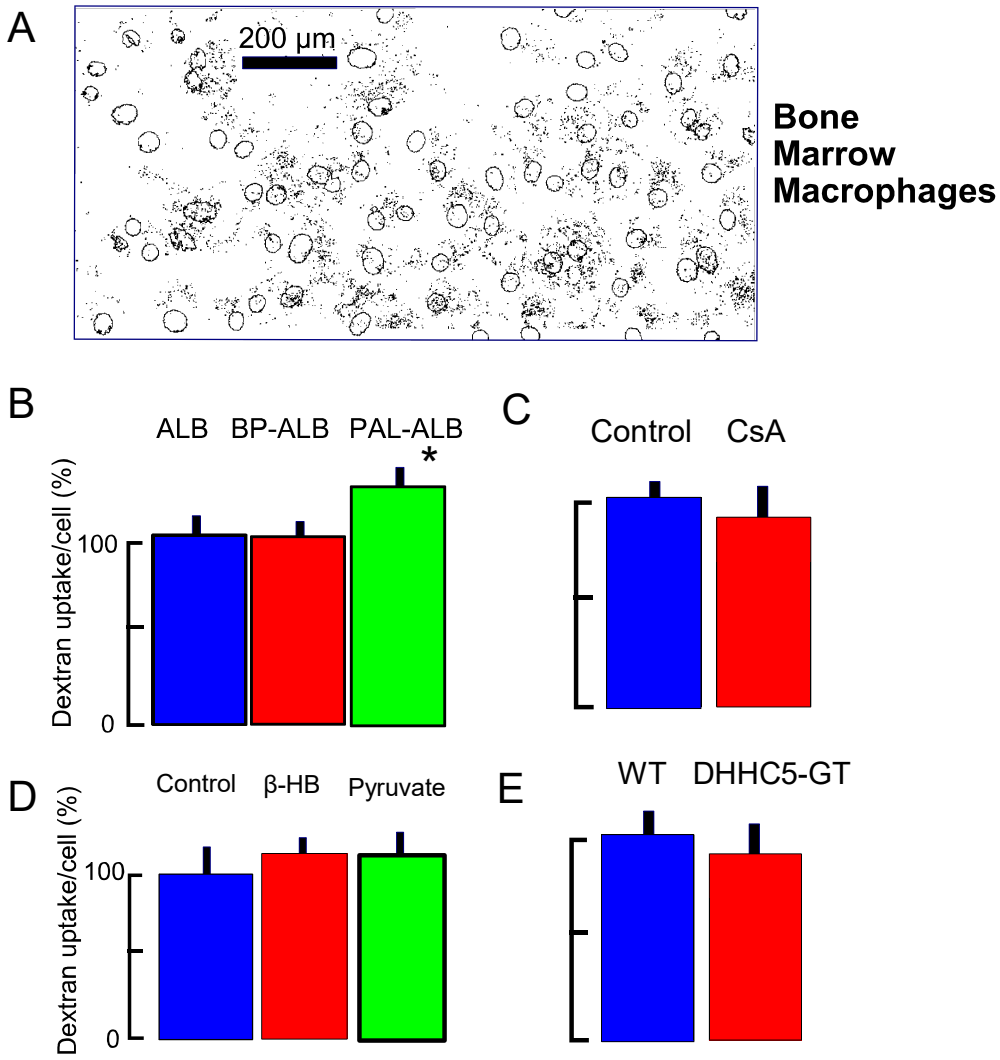
A
200 µm
Bone
Marrow
Macrophages
B
ALB
BP-ALB
PAL-ALB
*
Dextran uptake/cell (%)
100
0
C
Control
CsA
D
Control
β-HB
Pyruvate
Dextran uptake/cell (%)
100
0
E
WT
DHHC5-GT

Figure 11

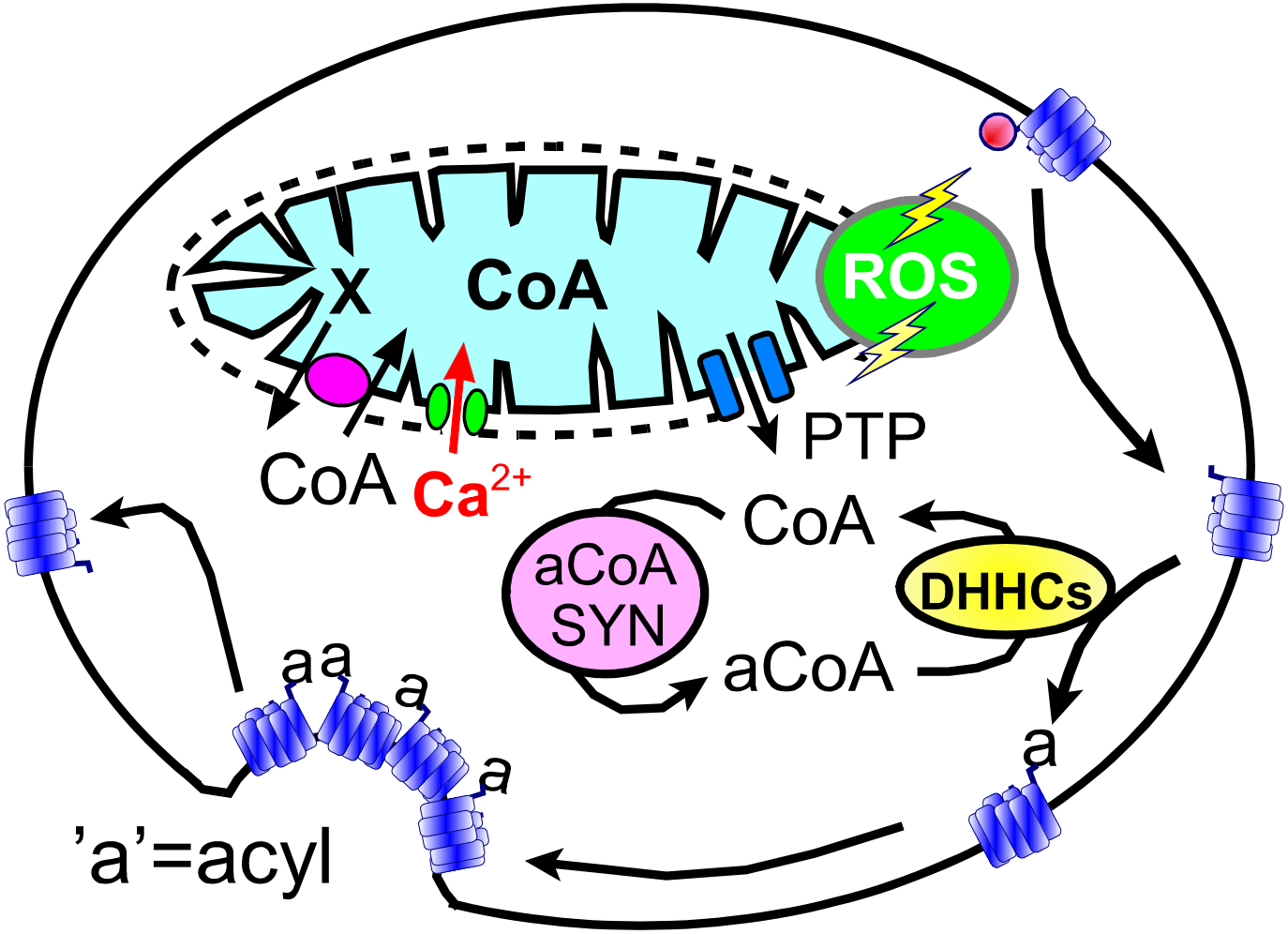

Figure 1

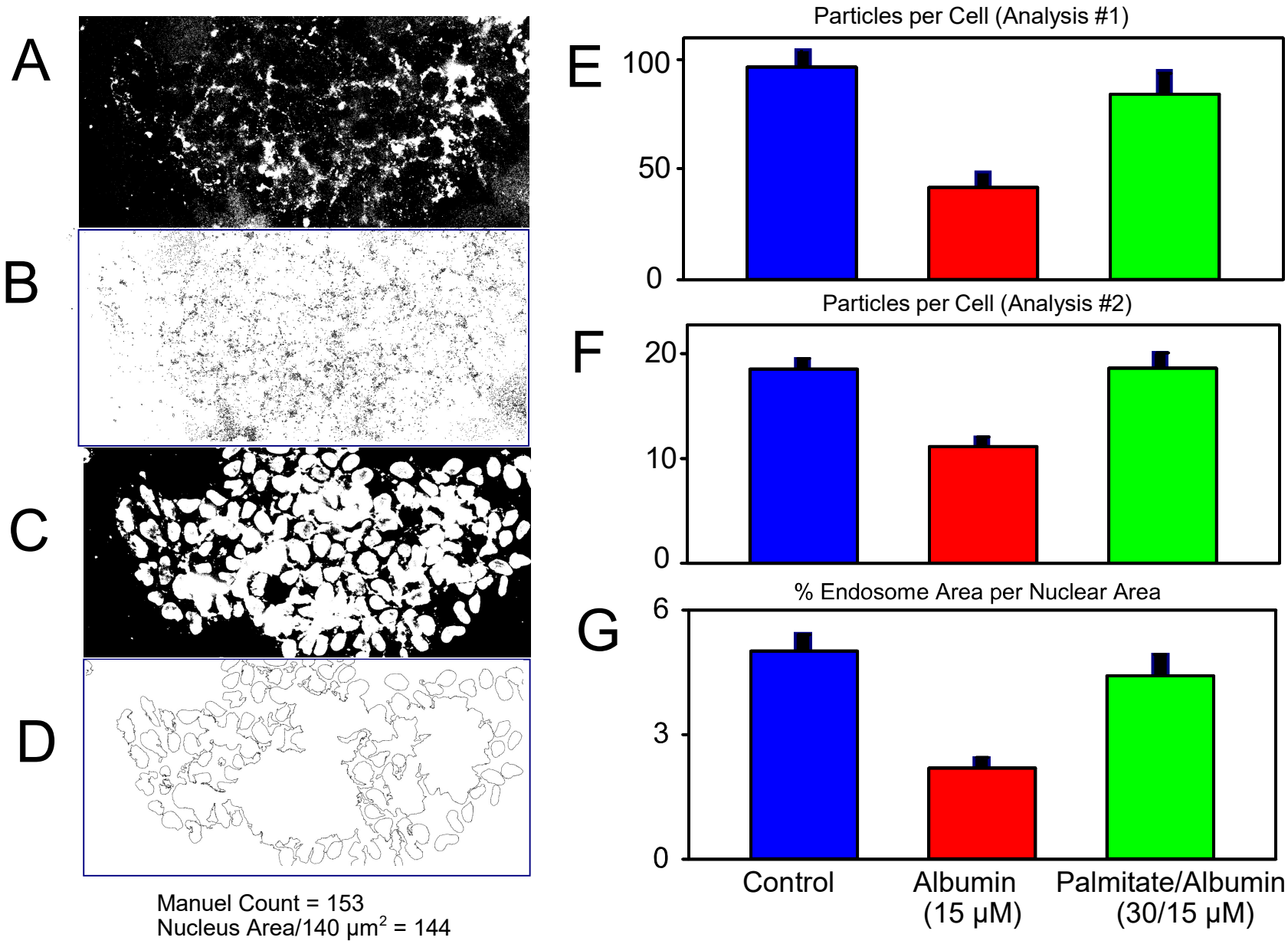
A
B
C
D
Manuel Count = 153
Nucleus Area/140 μm² = 144
E
Particles per Cell (Analysis #1)
100
50
0
F
Particles per Cell (Analysis #2)
20
10
0
G
% Endosome Area per Nuclear Area
6
3
0
Control
Albumin (15 μM)
Palmitate/Albumin (30/15 μM)

Figure 2

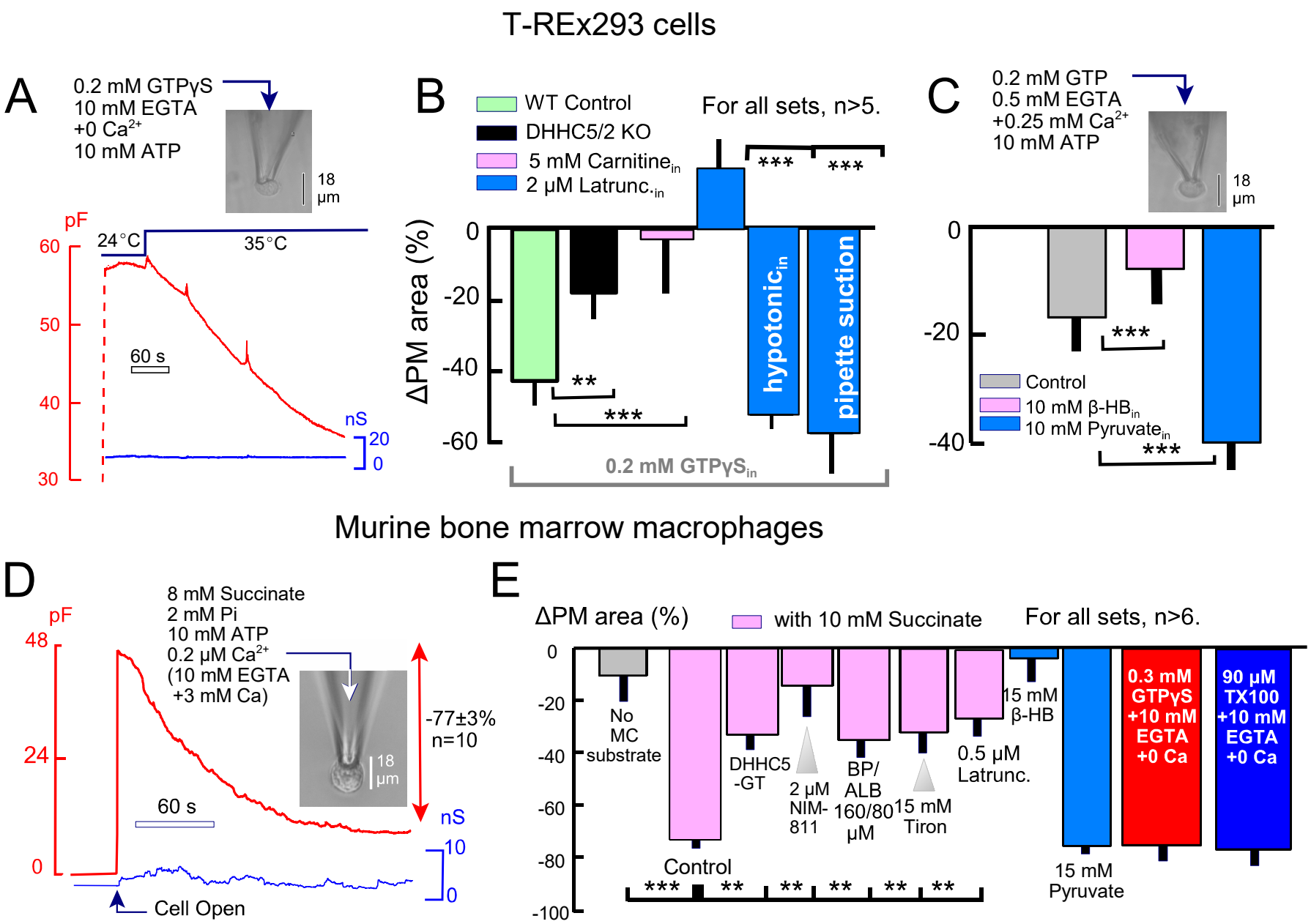
T-REx293 cells
A
0.2 mM GTPγS
10 mM EGTA
+0 Ca2+
10 mM ATP
18 µm
pF
60
50
40
30
24°C
35°C
60 s
nS
20
0
B
WT Control
DHHC5/2 KO
5 mM Carnitinein
2 µM Latrunc.in
For all sets, n>5.
ΔPM area (%)
0
-20
-40
-60
**
***
***
***
hypotonicin
pipette suction
0.2 mM GTPγSin
C
0.2 mM GTP
0.5 mM EGTA
+0.25 mM Ca2+
10 mM ATP
18 µm
0
-20
-40
***
***
Control
10 mM β-HBin
10 mM Pyruvatein
Murine bone marrow macrophages
D
8 mM Succinate
2 mM Pi
10 mM ATP
0.2 µM Ca2+
(10 mM EGTA
+3 mM Ca)
pF
48
24
0
18 µm
-77±3%
n=10
60 s
nS
10
0
Cell Open
E
ΔPM area (%)
with 10 mM Succinate
For all sets, n>6.
0
-20
-40
-60
-80
-100
No MC substrate
Control
DHHC5 -GT
2 µM NIM-811
BP/ ALB 160/80 µM
15 mM Tiron
0.5 µM Latrunc.
15 mM β-HB
15 mM Pyruvate
0.3 mM GTPγS +10 mM EGTA +0 Ca
90 µM TX100 +10 mM EGTA +0 Ca
***
**
**
**
**
**

Figure 3

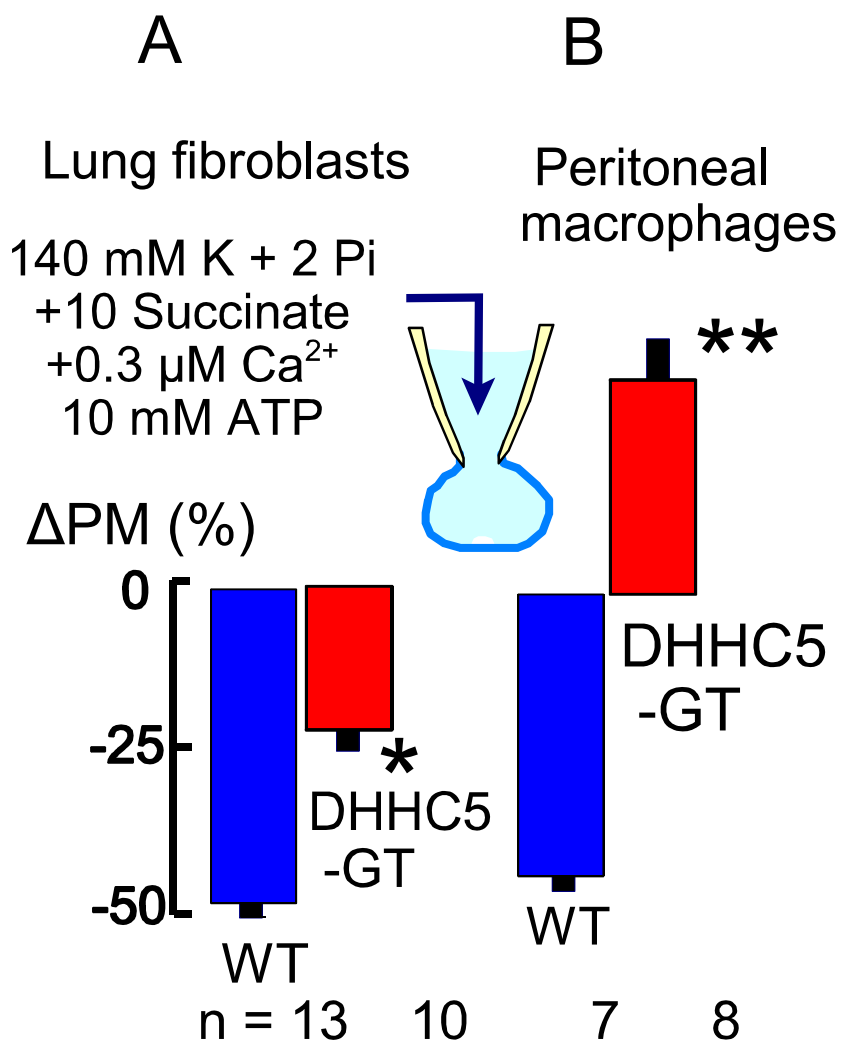
A
B
Lung fibroblasts
Peritoneal macrophages
140 mM K + 2 Pi
+10 Succinate
+0.3 μM Ca2+
10 mM ATP
ΔPM (%)
0
-25
-50
*
**
DHHC5 -GT
DHHC5 -GT
WT
WT
n = 13
10
7
8

Figure 4

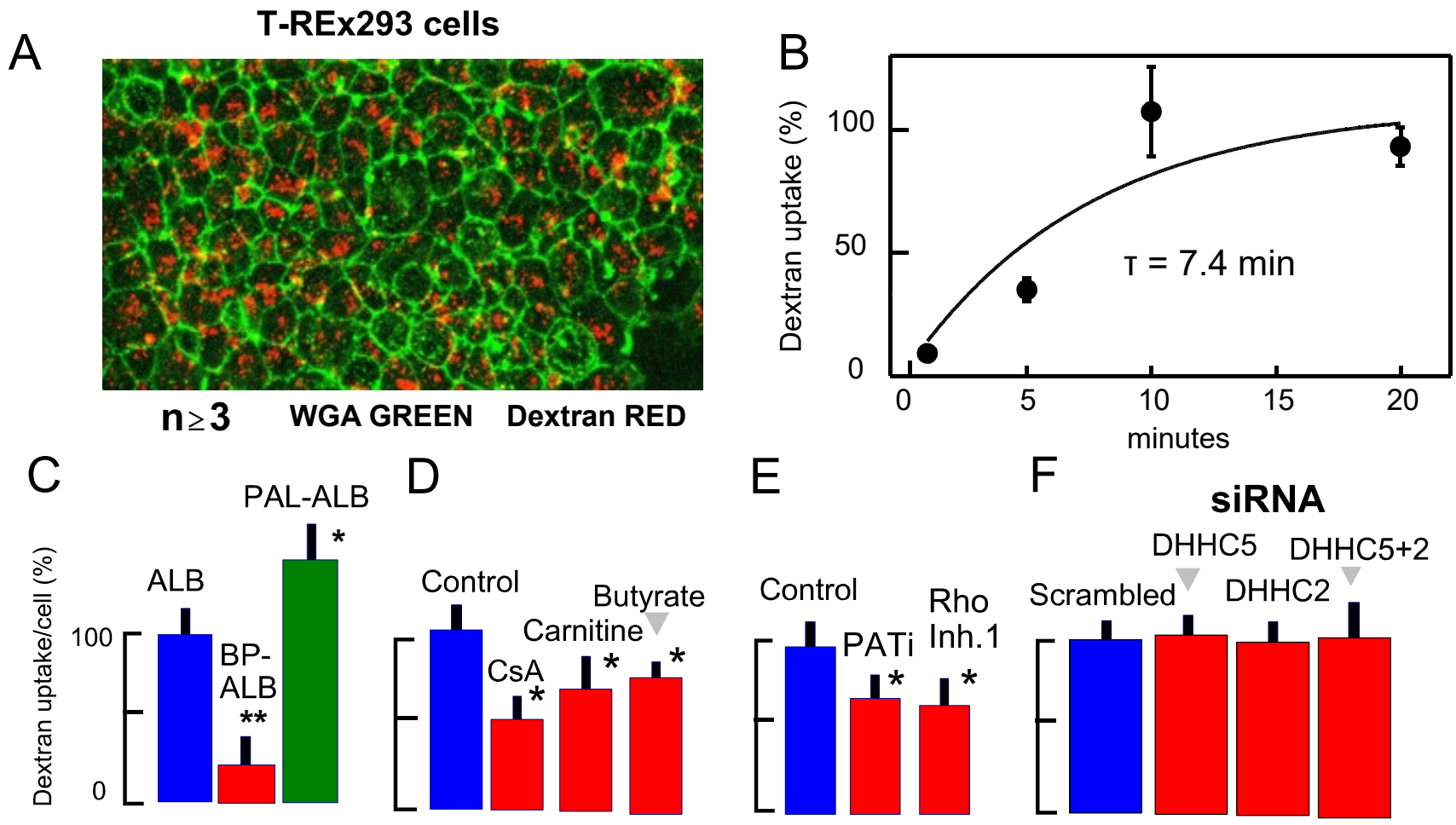
A
T-REx293 cells
n≥3
WGA GREEN
Dextran RED
B
Dextran uptake (%)
100
50
0
τ = 7.4 min
0
5
10
15
20
minutes
C
Dextran uptake/cell (%)
100
0
ALB
BP-ALB
PAL-ALB
**
*
D
Control
CsA
Carnitine
Butyrate
*
*
*
E
Control
PATi
Rho Inh.1
*
*
F
siRNA
Scrambled
DHHC5
DHHC2
DHHC5+2

Figure 5

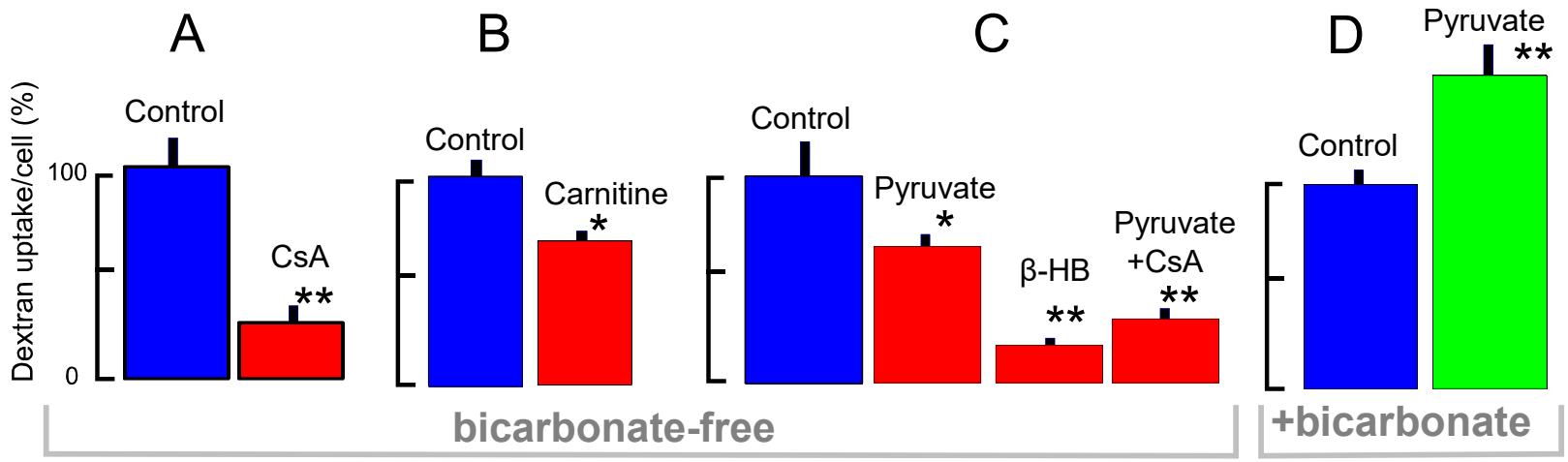
A
B
C
D
Dextran uptake/cell (%)
100
0
Control
CsA
**
Control
Carnitine
*
Control
Pyruvate
*
β-HB
**
Pyruvate
+CsA
**
Control
Pyruvate
**
bicarbonate-free
+bicarbonate

Figure 6

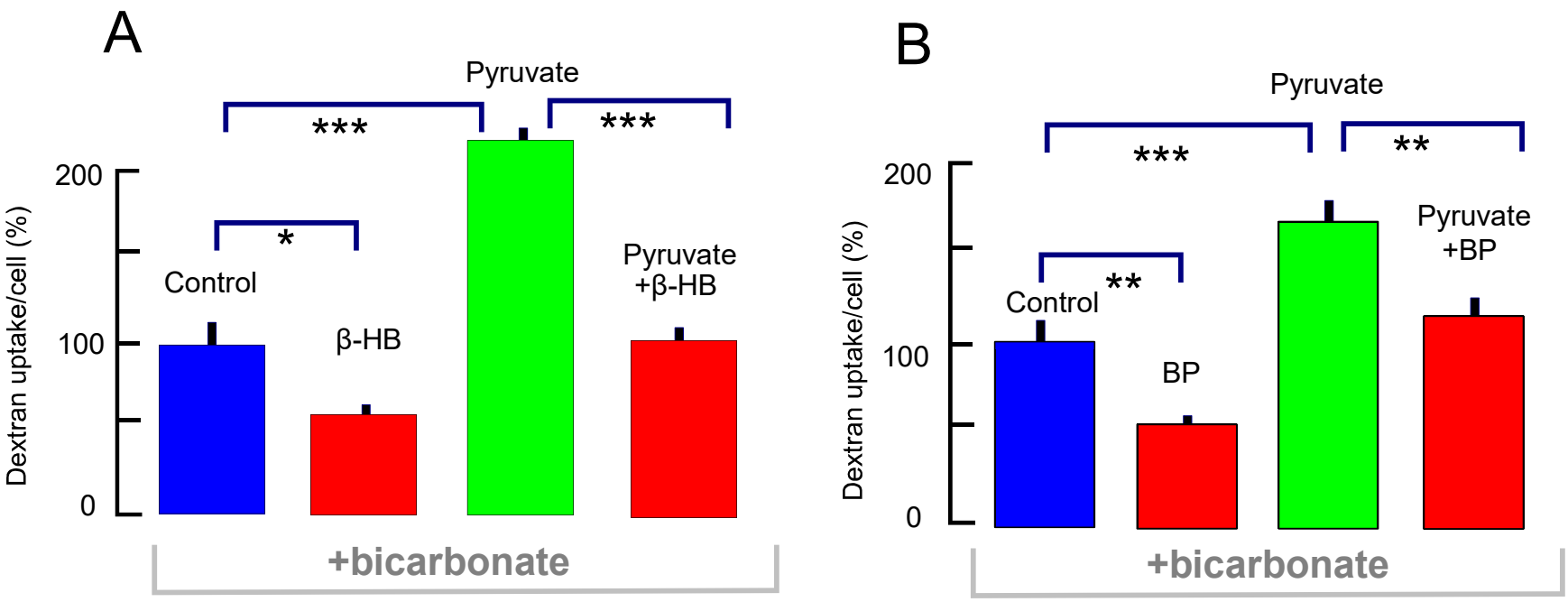
A
Pyruvate
***
***
*
200
100
0
Dextran uptake/cell (%)
Control
β-HB
Pyruvate
+β-HB
+bicarbonate
B
Pyruvate
***
**
**
200
100
0
Dextran uptake/cell (%)
Control
BP
Pyruvate
+BP
+bicarbonate

Figure 7

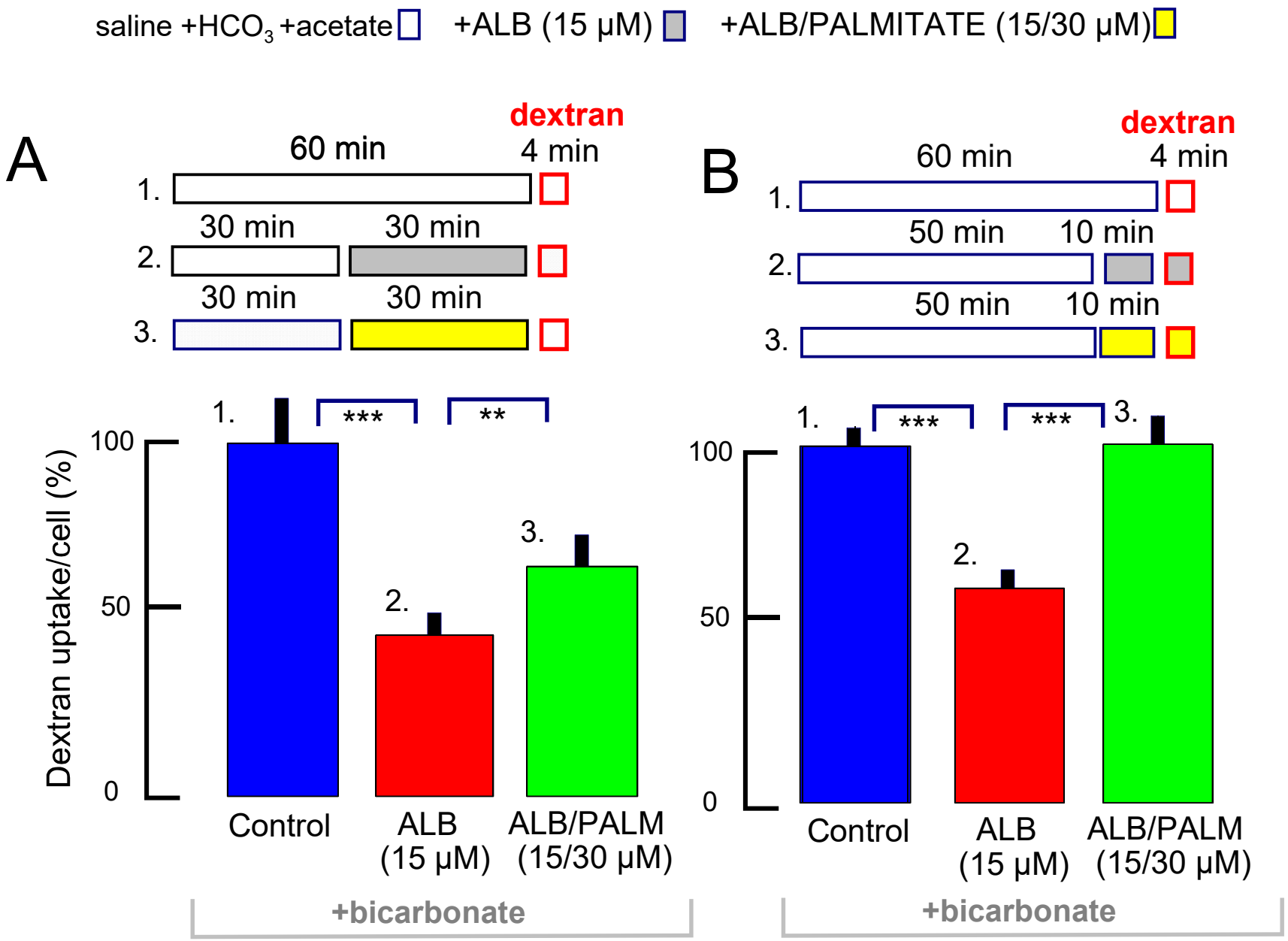
saline +HCO3 +acetate
+ALB (15 μM)
+ALB/PALMITATE (15/30 μM)
A
dextran
60 min
4 min
1.
30 min
30 min
2.
30 min
30 min
3.
Dextran uptake/cell (%)
100
50
0
1.
***
**
2.
3.
Control
ALB
(15 μM)
ALB/PALM
(15/30 μM)
+bicarbonate
B
dextran
60 min
4 min
1.
50 min
10 min
2.
50 min
10 min
3.
100
50
0
1.
***
***
3.
2.
Control
ALB
(15 μM)
ALB/PALM
(15/30 μM)
+bicarbonate

Figure 8

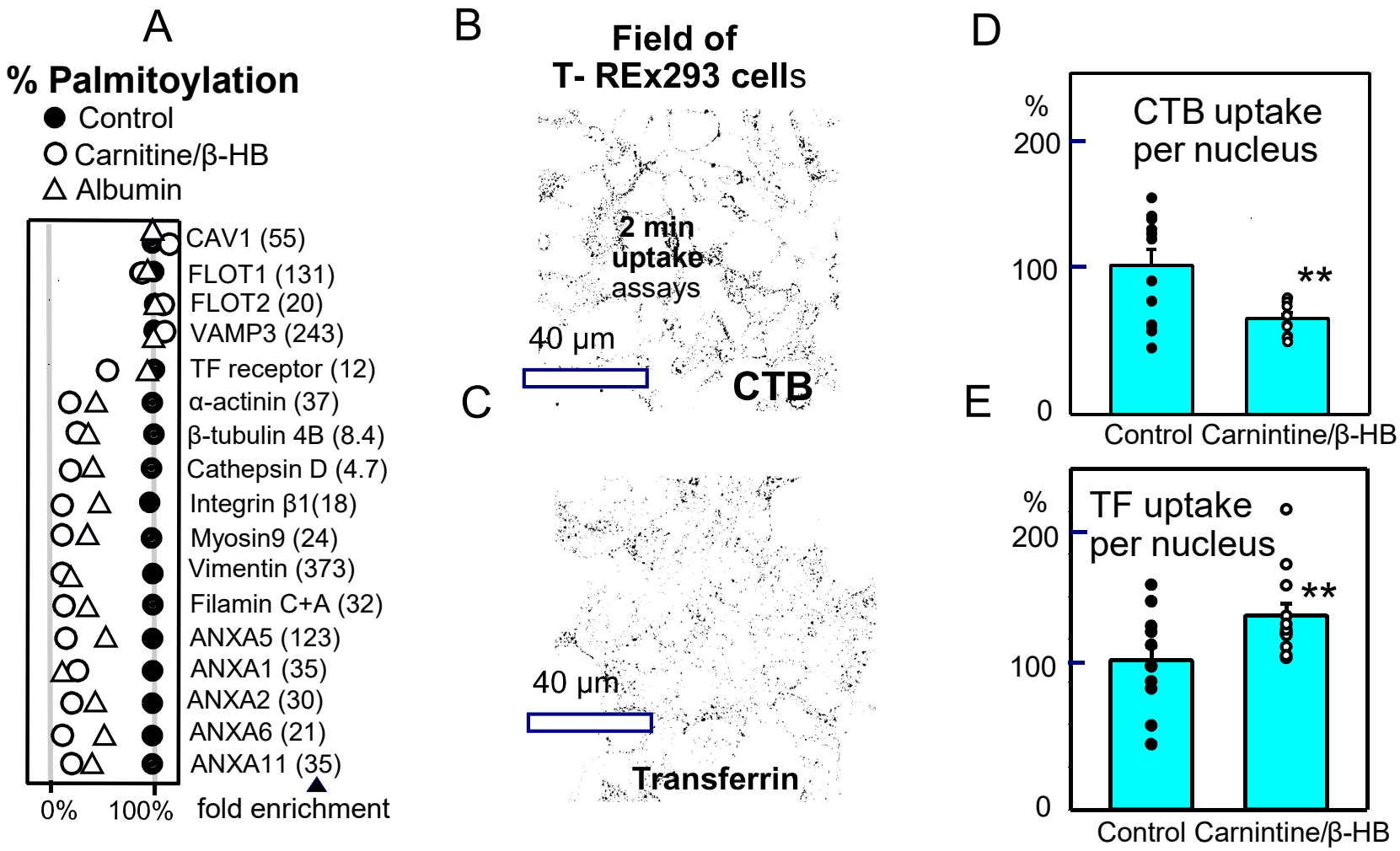
A
% Palmitoylation
Control
Carnitine/β-HB
Albumin
CAV1 (55)
FLOT1 (131)
FLOT2 (20)
VAMP3 (243)
TF receptor (12)
α-actinin (37)
β-tubulin 4B (8.4)
Cathepsin D (4.7)
Integrin β1(18)
Myosin9 (24)
Vimentin (373)
Filamin C+A (32)
ANXA5 (123)
ANXA1 (35)
ANXA2 (30)
ANXA6 (21)
ANXA11 (35)
0%
100%
fold enrichment
B
Field of
T- REx293 cells
2 min
uptake
assays
40 µm
CTB
C
40 µm
Transferrin
D
CTB uptake
per nucleus
%
200
100
0
**
Control
Carnintine/β-HB
E
TF uptake
per nucleus
%
200
100
0
**
Control
Carnintine/β-HB

Figure 9

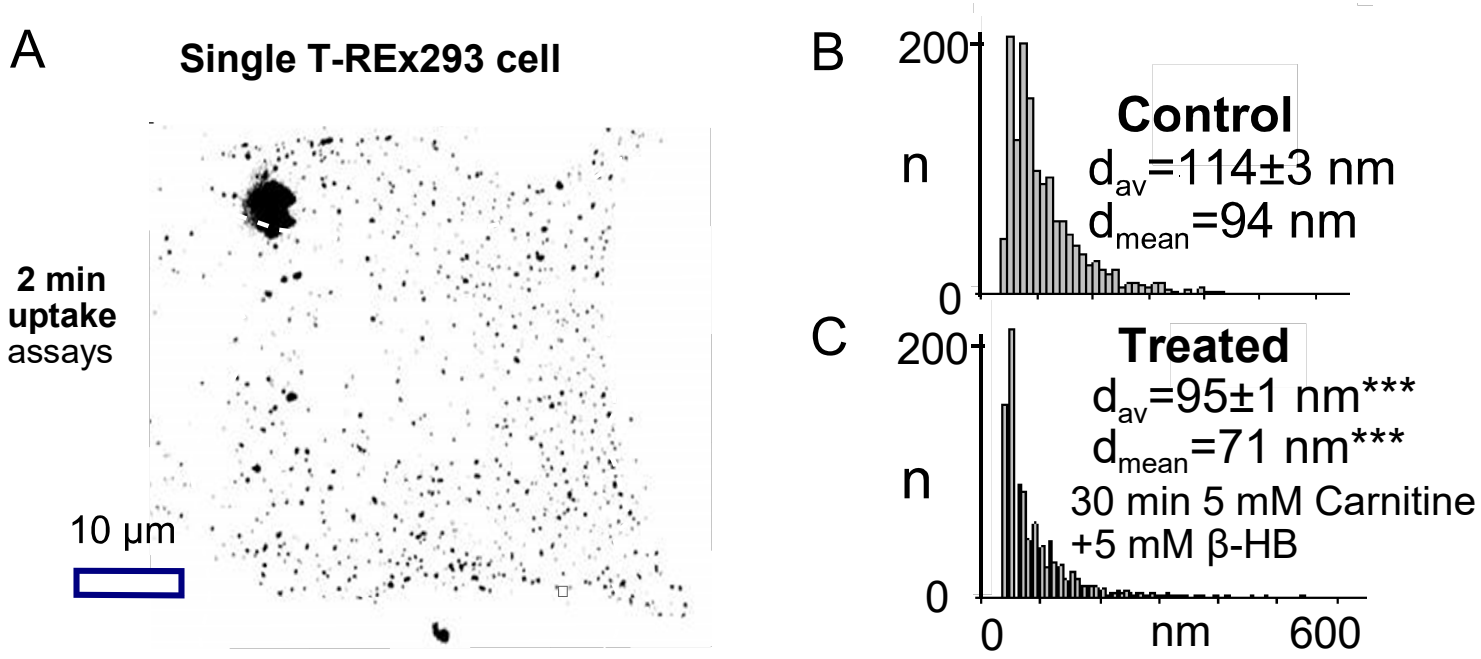
A
Single T-REx293 cell
2 min
uptake
assays
10 µm
B
200
n
0
Control
d_{av}=114±3 nm
d_{mean}=94 nm
C
200
n
0
Treated
d_{av}=95±1 nm***
d_{mean}=71 nm***
30 min 5 mM Carnitine
+5 mM β-HB
0
nm
600

Figure 10

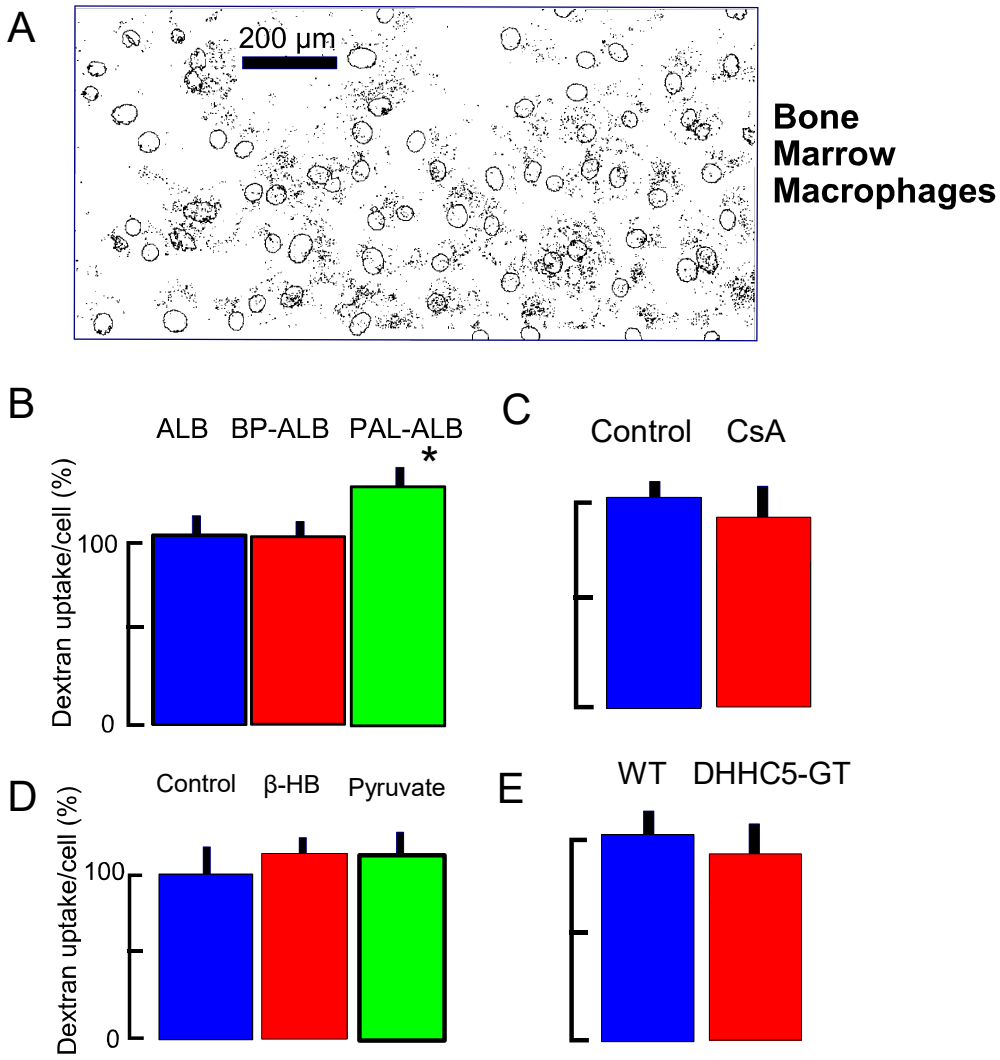
A
200 µm
Bone
Marrow
Macrophages
B
ALB
BP-ALB
PAL-ALB
*
Dextran uptake/cell (%)
100
0
C
Control
CsA
D
Control
β-HB
Pyruvate
Dextran uptake/cell (%)
100
0
E
WT
DHHC5-GT

Figure 11